AD_____

Award Number: W81XWH-05-1-0545

TITLE: Inhibitors for Androgen Receptor Activation Surfaces

PRINCIPAL INVESTIGATOR: Robert J. Fletterick, Ph.D.

CONTRACTING ORGANIZATION: University Of California, San Francisco
San Francisco, Ca 94143-0962

REPORT DATE: September 2007

TYPE OF REPORT: Annual

PREPARED FOR: U.S. Army Medical Research and Materiel Command
Fort Detrick, Maryland 21702-5012

DISTRIBUTION STATEMENT: Approved for Public Release;
Distribution Unlimited

REPORT DOCUMENTATION PAGE

Form Approved
OMB No. 0704-0188

1. REPORT DATE	2. REPORT TYPE	3. DATES COVERED
01-09-2007	Annual	1 Sep 2006 – 31 Aug 2007

4. TITLE AND SUBTITLE

Inhibitors for Androgen Receptor Activation Surfaces

5a. CONTRACT NUMBER

5b. GRANT NUMBER
W81XWH-05-1-0545

5c. PROGRAM ELEMENT NUMBER

6. AUTHOR(S)

Robert J. Fletterick, Ph.D.

Email: flett@msg.ucsf.edu

5d. PROJECT NUMBER

5e. TASK NUMBER

5f. WORK UNIT NUMBER

7. PERFORMING ORGANIZATION NAME(S) AND ADDRESS(ES)

University Of California, San Francisco
San Francisco, Ca 94143-0962

8. PERFORMING ORGANIZATION REPORT NUMBER

9. SPONSORING / MONITORING AGENCY NAME(S) AND ADDRESS(ES)
U.S. Army Medical Research and Materiel Command
Fort Detrick, Maryland 21702-5012

10. SPONSOR/MONITOR'S ACRONYM(S)

11. SPONSOR/MONITOR'S REPORT NUMBER(S)

12. DISTRIBUTION / AVAILABILITY STATEMENT
Approved for Public Release; Distribution Unlimited

13. SUPPLEMENTARY NOTES

14. ABSTRACT

Studies from this grant led to discovery of a new interaction site on the androgen receptor for binding proteins that regulate the function of the receptor. The protein binders have not been identified, but we showed that the site has the characteristics of functioning in repression. We used X-ray crystallography to discover the binding mode of four compounds that bind to this site. Their binding is accompanied by weakening the interaction of the androgen receptor with coactivators as shown by disorder or representative peptides that were well ordered before adding the compounds. Thus, atomic level imaging of these interactions fit with the notion that the site functions in repression, as suggested by analysis of mutations of amino acid residues found in humans in cell and biochemical assays. This work suggests that compounds may be designed to target this site and weaken activity of the androgen receptor. Such compounds could form a new class of chemical therapeutics for treatment of prostate cancer.

15. SUBJECT TERMS
X-ray crystallography, high throughput screening, medicinal chemistry

16. SECURITY CLASSIFICATION OF:			17. LIMITATION OF ABSTRACT	18. NUMBER OF PAGES	19a. NAME OF RESPONSIBLE PERSON
a. REPORT	b. ABSTRACT	c. THIS PAGE			19b. TELEPHONE NUMBER *(include area code)*
U	U	U	UU	37	USAMRMC

Standard Form 298 (Rev. 8-98)
Prescribed by ANSI Std. Z39.18

Table of Contents

INHIBITORS FOR ANDROGEN RECEPTOR ACTIVATION SURFACES
Contract: W81XWH-05-1-0545
R. Fletterick, P.I.
Department of Defense Progress Report 2007
Period 9.1.06-8.31.07

INTRODUCTION

Androgen receptor (AR) regulates gene expression required for early prostate cancer growth and survival. In early stage cancer, AR activity caused by endogenous androgens promotes the disease. Fortunately, AR action can be blocked by hormone withdrawal or with antiandrogens that compete for the hormone-binding site within the AR ligand binding domain (LBD). Unfortunately, in tumor progression secondary events (including AR mutations or modifications and alteration in AR and cofactor levels) sensitize AR action to low androgen or antiandrogen environments, thereby reactivating AR dependent gene expression programs and leading to proliferation of tumors. Eventually these evolve resistance to existing chemotherapeutics that inhibit by competition for the hormone binding pocket. An alternative class of inhibitors, which bind to NR surfaces that mediate assembly of the receptor's binding partners, might slow the route to advanced disease. We conducted two types of screens to identify surface binding compounds; functional and structural by X-ray crystallography. We expected to directly block AR activation function 2 (AF-2), which is hormone directed formation of an AR surface to bind coactivators. The so called AF-2 pocket is characterized at atomic level. Four compounds- three nonsteroidal anti-inflammatories (NSAIDs) and the thyroid hormone, Triac were found to block coactivator binding in solution with $IC_{50} \approx 50\mu M$. Most importantly, inhibition of AF-2 activity by these four was detected in cells. X-ray analysis of compounds at the AR surface confirms weak binding at AF-2. A major surprise showed that the most potent inhibitors bind preferentially to a previously unknown cleft termed binding function-3 (BF-3). A search of the human mutation database showed mutations at BF-3 linked to prostate cancer and androgen insensitivity syndrome. X-ray analysis revealed a possible mechanism. The compound Triac binds to BF-3 with apparent conformational changes at the adjacent interaction site AF-2. The experiments imaged a much less ordered (weaker binding) coactivator peptide at AF-2. We used functional assays to show that mutation of residues that form BF-3 inhibits AR function and AR AF-2 activity. We propose that BF-3 is a previously unrecognized allosteric regulatory site needed for AR activity *in vivo* and a possible pharmaceutical target.

BODY

Original Objectives and Specific Aims

Our objective is to synthesize molecules that bind AR AF-2 (or other protein interaction surfaces) and inhibit assembly of AR/coactivator complexes. These compounds could comprise new leads in our search for therapies for primary and secondary prostate cancer.

Aim 1: X-ray Screening of Fragments. Soak AR crystals in mixtures of drug-like fragments that are about 200 Daltons and contain sites for later coupling reactions with linkers to combine fragments. Determine three dimensional structures of soaked crystals to locate compounds on the AR surface.

Aim 2: Focused Chemistry. Assemble libraries of computationally designed compounds that will fill the defined sub-pockets in the AF-2 surface. Soak AR crystals in mixes of these compounds and use X-ray crystallography to locate binding compounds, as described for Aim 1.

Aim 3: Identification and Characterizations of Bound Molecules. Positive binding compounds will be identified by direct imaging from Aims 1 and 2, or by deconvolution and additional crystal soaks to determine high resolution structures of compounds attached to AR. Binding interactions and constraints on additions to the bound fragment will be characterized from atomic coordinates.

Aim 4: Linkage Chemistry and Assays. Identified fragments from Aim 1 will be linked by synthetic chemistry to make compounds that will be tested for binding in biochemical and cell assays and by X-ray crystallography. Lead compounds identified in Aim 2 will be tested using the same methodologies.

SUMMARY OF RESULTS

Aims 1 and 2 were completed with compound libraries that included about 3000 compounds.
Aim 3 was completed using X-ray crystallography to image the identity of bound compounds and provide a qualitative degree of binding affinity. The results for Aims 1 through 3 was identification of 7 compounds binding at two surface sites, with 4 compounds binding tightly and 3 binding weakly Kd ~ 1-5 mM.

Binding Function 3 (BF3) is a Surface on the Androgen Receptor that Allosterically Regulates Coactivator Binding. This is a major result. We proved that interactions at BF-3 weaken coactivator binding (Fig 1). Comparison of the AR surface +/- Triac, T_3 and FLF reveals structural alterations. Four BF-3 residues (Arg840, Asn727, Phe826 and Glu829) that point out of the pocket into solution point inwards and engage the compound (Fig. 3A). This is accompanied by large movements of the Arg726 side chain, close to AF-2, and repositioning of AF-2 residues Lys717 and Met734 (not shown). Small but significant shifts in secondary structural elements; residues 720-730 (H3) and 825-847 (H9) exhibit root mean square deviation (r.m.s.d) of 0.33 and 0.44, are observed but not interpreted mechanistically. Thus, Triac and FLF promote structural rearrangements in BF-3 that are propagated to AF-2.

Strikingly, interactions at BF-3 disorder coregulator peptides that are bound to AF-2. In crystals of ternary complexes of AR LBD-DHT-SRC2-3 (LXXLL) and AR LBD-DHT-ARA70 (FXXLF), the peptides fold into α-helices of 15 and 9 amino acids (20), respectively, clearly defined by electron density (Figs. 3A, 3B, insets). Short incubations with Triac result in loss of electron density in regions flanking SRC2-3 (Fig. 5A, and inset) and disruption of Arg726 interactions with SRC2-3 residues that lie C-terminal to the LxxLL motif. Triac binding to BF-3 also weakened contacts to the second class of coactivator, represented by ARA70 with motif FxxLF (Fig. 3B); only four residues are visible with Leu+4 and Phe+5 completely defined (Fig. 3B, inset). Arg726 does not contact the FXXLF peptide, suggesting that reorganization of AF-2 itself is important for this effect. Unexpectedly, Arg840 adopts the inwards facing conformation in this experiment (Fig. 3B). Similar Arg840 rearrangements are also seen with artificial FXXLF peptides, suggesting that it is a hitherto unappreciated feature of AR interactions with these NR boxes. It is unlikely that Triac interacts directly with AF-2 to disrupt coactivator binding; it is not detected at AF-2 at these times and the electron-rich iodine groups of Triac representing particularly good markers. Control soaks with solvent (DMSO) reveal no similar effects on coregulator peptide organization (not shown). Thus, Triac interactions at BF-3 weaken contacts between AR and coactivator peptides.

Functional analysis of Binding Function 3:
If BF-3 is important for AR action, then BF-3 mutations should alter AR activity. Mutations at Gln670, Ile672 and Leu830 in the BF-3 groove are associated with prostate cancer, where they enhance AR function. Leu830, Pro723, Gly724, and Arg840 in BF-3 are mutated in androgen insensitivity syndrome,

(http://www.androgendb.mcgill.ca/). Targeted mutagenesis of Asn727 and Arg840, which move on Triac binding, eliminate AR-LBD activity (Fig. 3C), similar to the degree of inhibition obtained with mutations in AF-2. Likewise, mutations at Phe673, Pro723, Glu724 and Glu737 and, possibly, Arg 726 and Phe826 reduce activity. Mutations in nearby residues, including Gln670, Ile672, Glu829 and Asn833, increase AR AF-2 activity up to five fold. Similar results are obtained with full length AR at MMTV-LUC; mutations at Phe673, Pro723 and Arg840 inhibited androgen response (Fig. 3D). Together, mutations that inhibit AR activity describe a continuous patch that resembles the BF-3 surface defined by chemical interactions (Fig. 3E).

BF-3 could be present in other NRs. Part of the BF-3 site; the loop between helices 3 and 4 is a signature sequence. BF-3 residues are conserved in the steroid subfamily, as superposition of their published structures reveals (Fig. 4). Mutations in equivalent regions of estrogen and glucocorticoid receptor are implicated in coactivator binding. Collectively, these data provide evidence for a role of BF-3 in NR action in health and disease.

Fig. 1. *Location of AF-2 and BF-3.* A Schematic of AR LBD showing the location of the DHT, key AF-2 helices (3,5, and 12) and H1. B Space filling model of AR LBD showing key residues in AF-2 (cyan) and BF-3 (red). C. As in Fig. 3B, but rotated 90^{o} to reveal BF-3.

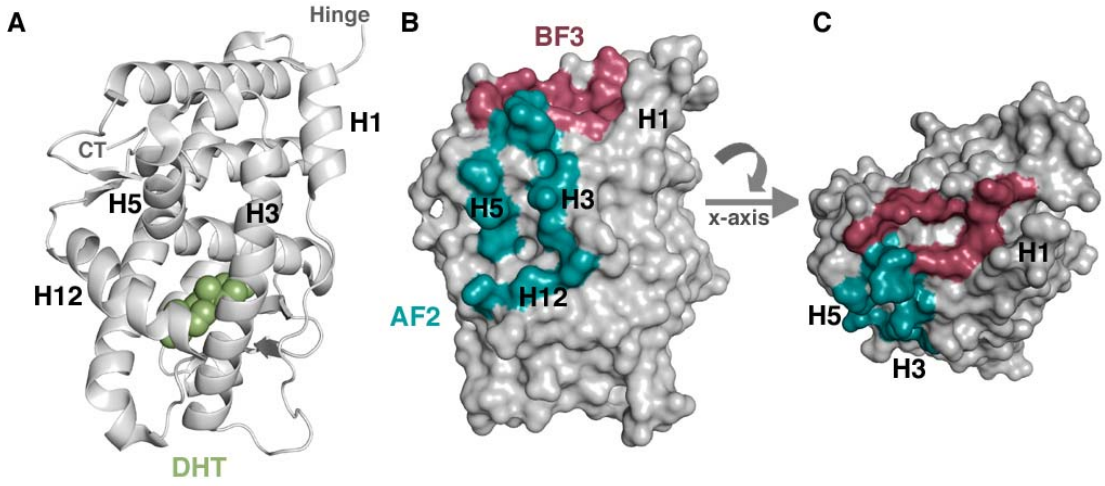

Fig. 2. *Small Molecules inhibit coregulator binding and AR AF-2 activity.* (A-B) Dose response analysis using fluorescence polarization of (A) TOL and (B) Triac in the presence of AR LBD and fluorescent peptide SRC2-3. (C) SDS-PAGE showing *in vitro* translated SRC2 retained in pulldowns with AR-LBD/DHT complex with vehicle (0), 10μg SRC2-3 peptide or FLF (1, 3, 10, 30, 100 μM). (D, E) AR AF-2 transcription readouts in HeLa. Components are shown in schematic at the top. Panels show luciferase assays (light units x 10^4) normalized to β-galactosidase. Standard errors are derived from sextuplet points. Experiments were performed with similar results five times. (F) AR transcription readouts. Components are shown in schematic at top. The figure represents a typical experiment with DHT response set to 100%.

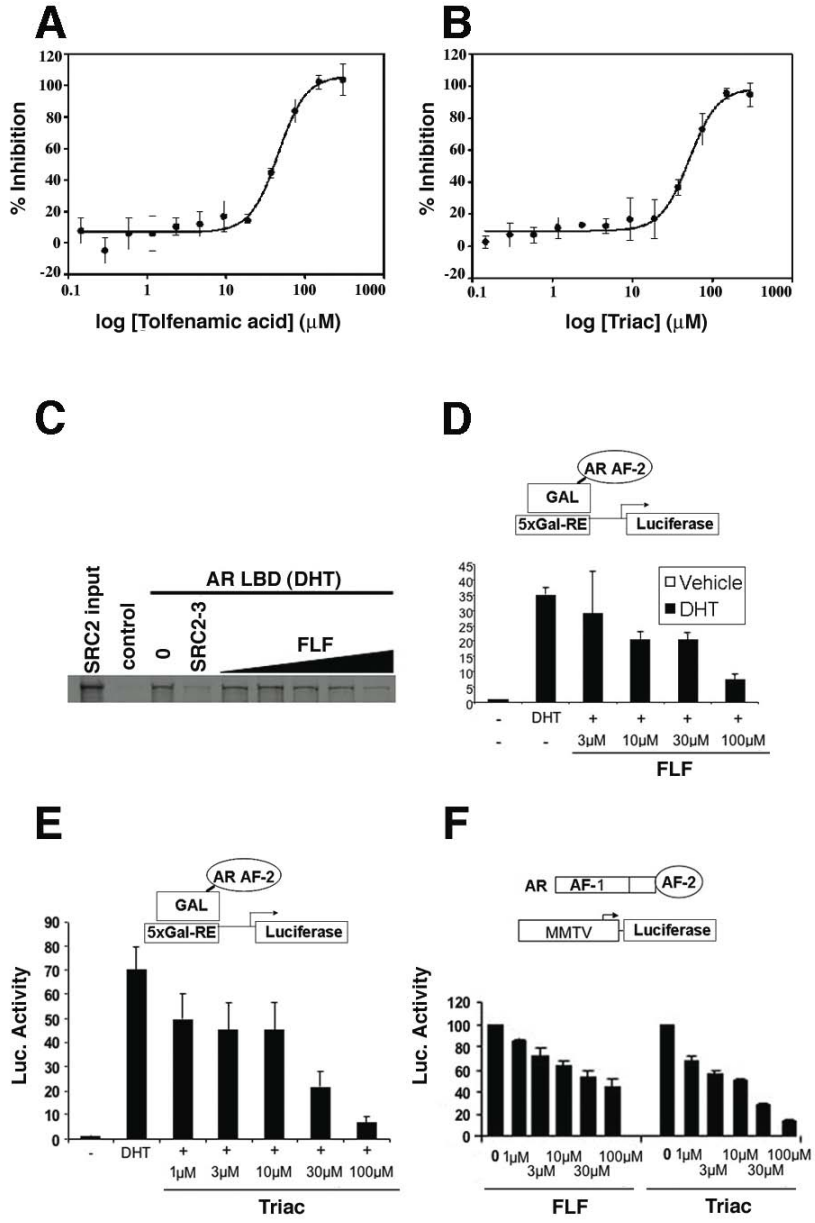

Fig. 3. *BF-3 is an allosteric regulator of AF-2*. (A) Superposition of AR with 15*mer* SRC2-3 + (blue sticks) and - Triac (gray sticks) and + Triac with no peptide (yellow sticks). Arg840, Phe826, Asn727 (BF-3) and Arg726 (AF-2) adopt different conformations. Without Triac, Arg840 points outward and Arg726 contacts SRC2-3 (gray). With Triac, Arg840 contacts ligand and Arg726 does not contact SRC2-3 (blue). Right panel shows SRC2-3 at AF-2 without (gray α-trace) and + Triac (blue α-trace). Blue dots indicate regions not visible with Triac; Leu residues as sticks. (B) As above, with 15*mer* ARA70 \ + (blue) and - Triac (gray). Reorganization is similar to (A) except that Arg840 points inwards without Triac. (C) AR AF-2 assay; wild type AR = 100%. Results are averages of multiple experiments n>3. (D) Representative transfection with full length AR active at MMTV-Luc. (E) BF-3 defined by mutagenesis. Residues needed for activity in raspberry; mutations that increase activity in green.

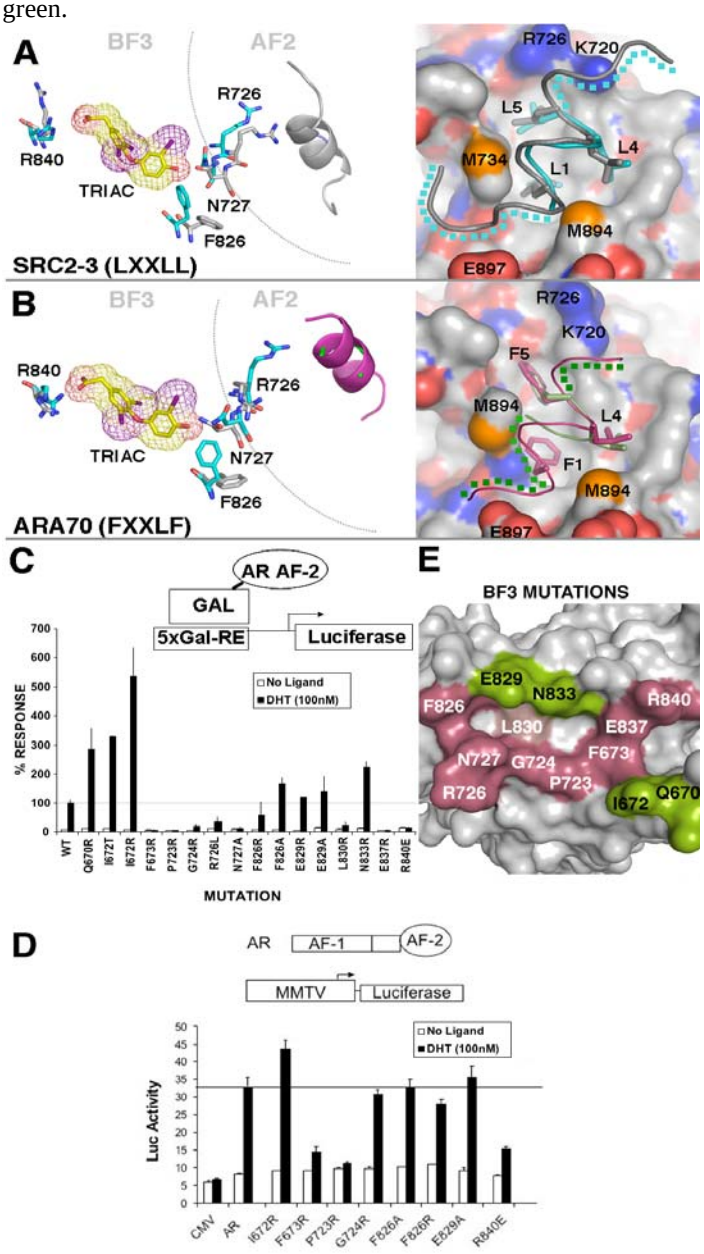

KEY RESEARCH ACCOMPLISHMENTS

- Four compounds were found that bind to surfaces of the human androgen receptor. Cell assays showed that these compounds inhibit transcription in cells in the context of a LBD driving a reporter or of full length AR driving a reporter. Thus, screens developed by this grant led to new compounds that may be chemotypes for new classes of AR inhibitors.

- Discovery of an allosteric effector site of the androgen receptor that has characteristics of a repressor function. Binding at BF3 alters structure disordering coregulator domains bound at AF-2.

REPORTABLE OUTCOMES

Patents

Submitted application: SF2007-128 "Allosteric Effectors of Androgen Receptor"
R. Fletterick, E. Estebanez-Perpina, John D. Baxter, Kip Guy (2007)
UCSF Office of Technology Management (OTM). Not pursued per UCSF OTM, 2007)
The invention relates to the identification and characterization of a novel regulatory surface on the AR LBD (BF3 pocket) and allosteric coactivator modulators and will be reactivated when second generation compounds are obtained. The chemistry needed to develop second generation compounds will require additional funding.

Publications

1. Estébanez-Perpiñá, E., Arnold, L.A., Mar, E., Bateman, R., Shokat, K., Guy, R. K. and Fletterick, R.J. Inhibitors of Androgen Receptor-Coregulators Assembly. *Proc Natl Acad Sci U S A* (*PNAS*), Oct 9;104(41):16074-9. Epub 2007 Oct 2. PMID: 17911242 [PubMed - in process]

2. Estébanez-Perpiñá, E., Arnold, L.A., Jouravel, N., Togashi, M., Blethrow J., Mar, E., Nguyen P., Phillips K.J., Baxter, J.D., Webb, P., Guy, R. K. and Fletterick, R.J. Structural Insight into the Mode of Action of a Direct Inhibitor of Coregulator Binding to the Thyroid Hormone Receptor.. *Molecular Endocrinology,* 2007 Sep 6; [Epub ahead of print] PMID: 17823305 (related to screening concepts for AR and confirms idea of surface interacting drugs)

3. Estébanez-Perpiñá, E., Jouravel, N., and Fletterick, R.J. Perspectives on Designs of Anti-Androgens for Prostate Cancer. Expert Opinion in Drug Discovery, in press, October 2007.

4. Estébanez-Perpiñá, E., Arnold, L.A., Baxter, J.D., Webb, P., Guy, R. K. and Fletterick, R.J. Developing therapeutic agents for androgen-independent prostate cancer. Invited review Nuclear Receptor Signaling (NURSA), in press, Sept. 2007.

5. Estébanez-Perpiñá, E., and R.J. Fletterick. The Androgen Receptor Coactivator Binding Interface. Invited book chapter by Springer Science. In preparation, Sept. 2007.

CONCLUSIONS

We screened chemical libraries of compounds with two strategies to identify organic molecules that bind to the AR LBD surface. Most of the ~1100 compounds tested belong to a commercial library of FDA-approved bioavailable drugs. The first strategy used a fluorescently labeled coregulator peptide known to bind to the AR AF2 site; the second exploited X-ray crystallography to discover organic molecules that bind at the surface of the AR LBD in crystals. The first approach identified four compounds that blocked peptide coactivator recruitment: thyroid hormone analogue 3,3',5-triiodothyroacetic acid (TRIAC), and three aspirin-derivatives flufenamic acid, tolfenamic acid, and meclofenamic acid. The X-ray strategy identified six compounds, four of them bound to AF2: 2-methylindole (2MI), 1-tert-Butyl-3-(2,5-dimethyl-benzyl)-1H-pyrazolo[3,4-d]pyrimidin-4-ylamine (K10), 3-((1-tert-butyl-4-amino-1H-pyrazolo[3,4-d]pyrimidin-3-yl)methyl)phenol (RB1) and T3 hormone.

The most important discovery of this project is finding a site we called BF3. TRIAC, T3 hormone, flufenamic acid, 2MI and indole-3-carboxylic acid bind to this locus. Thus, using complementary approaches, we identified small molecules that target the coactivator-binding pocket and BF3 site of AR. The identification of binding molecules and accompanying three-dimensional structures may be used to develop tighter and more specific lead molecules.

Plans for further work: We are using 2-hybrid screens to identify the endogenous proteins that bind to BF3.

A surface on the androgen receptor that allosterically regulates coactivator binding

Eva Estébanez-Perpiñá*, Alexander A. Arnold†, Phuong Nguyen‡, Edson Delgado Rodrigues‡, Ellena Mar*, Raynard Bateman§, Peter Pallai¶, Kevan M. Shokat§, John D. Baxter‡‖, R. Kiplin Guy†, Paul Webb‡, and Robert J. Fletterick*‖

*Department of Biochemistry and Biophysics, §Department of Molecular and Cellular Pharmacology, and ‡Diabetes Center and Department of Medicine, University of California, San Francisco, CA 94143; †Department of Chemical Biology and Therapeutics, St. Jude Children's Research Hospital, Memphis, TN 38105; and ¶Bioblocks, Inc., San Diego, CA 92121

Contributed by John D. Baxter, August 24, 2007 (sent for review May 12, 2007)

Current approaches to inhibit nuclear receptor (NR) activity target the hormone binding pocket but face limitations. We have proposed that inhibitors, which bind to nuclear receptor surfaces that mediate assembly of the receptor's binding partners, might overcome some of these limitations. The androgen receptor (AR) plays a central role in prostate cancer, but conventional inhibitors lose effectiveness as cancer treatments because anti-androgen resistance usually develops. We conducted functional and x-ray screens to identify compounds that bind the AR surface and block binding of coactivators for AR activation function 2 (AF-2). Four compounds that block coactivator binding in solution with $IC_{50} \approx 50$ μM and inhibit AF-2 activity in cells were detected: three nonsteroidal antiinflammatory drugs and the thyroid hormone 3,3′,5-triiodothyroacetic acid. Although visualization of compounds at the AR surface reveals weak binding at AF-2, the most potent inhibitors bind preferentially to a previously unknown regulatory surface cleft termed binding function (BF)-3, which is a known target for mutations in prostate cancer and androgen insensitivity syndrome. X-ray structural analysis reveals that 3,3′,5-triiodothyroacetic acid binding to BF-3 remodels the adjacent interaction site AF-2 to weaken coactivator binding. Mutation of residues that form BF-3 inhibits AR function and AR AF-2 activity. We propose that BF-3 is a previously unrecognized allosteric regulatory site needed for AR activity *in vivo* and a possible pharmaceutical target.

antagonist | high-throughput screening | regulatory surface | antiandrogens | nuclear receptors

Nuclear receptors (NRs) play widespread roles in disease and are major targets for pharmaceuticals (1), with many new compounds in development (2). Most NR ligands interact with the internal ligand binding pocket [binding function (BF) 1] in the C-terminal ligand binding domain (LBD) core (3). From here, the ligands modulate NR activity by allosterically reshaping the LBD surface, with concomitant effects on coregulator association and gene expression (3–6). It remains conceivable that ligands could bind elsewhere. We identified a compound that binds to the TR dimer interaction surface (7), we and others identified compounds that bind the NR activation function 2 (AF-2) surface (discussed below), and another group showed that glucose and oxysterols cooperate in activation of liver X receptors (8).

The strategy of targeting the ligand binding pocket with pharmaceuticals has limitations. First, ligand size can be limited by the enclosed nature of the pocket (3). Second, it is difficult to devise strategies to modulate interaction surfaces that are not remodeled by ligand or orphan NRs that lack known ligands or ligand binding cavities. Third, partial agonist or mixed agonist activities of ligands that bind BF-1 may not be desirable. This is a particular problem for androgen receptor (AR) and estrogen receptor antagonists, which are used to treat, respectively, hormone-dependent prostate and breast cancers but can become ineffective and promote tumor growth (9–11).

In principle, pharmaceutical attack at NR surface active sites could overcome these problems (12), and NR AF-2 is a particularly attractive drug target (13). AF-2 is formed in response to agonist binding and binds coregulators, including the steroid receptor coactivator (SRC) family. Only 6–8 amino acids in AF-2 are crucial, and these form a hydrophobic cleft that binds short α-helical peptides (NR boxes) in target coactivators and could bind small molecules (BF-2). We identified two compounds that block thyroid hormone receptor AF-2 association with coactivators in solution and receptor activity in cells (14). Others identified estrogen receptor-interacting compounds, some of which block coregulator binding *in vitro* (14–17).

Strategies that target AR AF-2 could yield new therapeutics for prostate cancer and other conditions (18–22). AR AF-2-interacting peptides inhibit androgen response, representing proof of principle that intervention at this surface is a viable strategy for inhibition of AR activity *in vivo* (18). Compounds that bind AF-2 should inhibit intramolecular association between the AR LBD and N-terminal domain (23) required for optimal AR responses at many target genes and interactions with coregulators that participate in AR action such as AR-associated protein 70 (ARA70) and SRC2 (20). AR AF-2 binds short α-helical peptides with consensus FXXLF and the more common NR consensus LXXLL. Our x-ray structures of AR LBD with representative peptides reveal that AF-2 amino acid side chains move to create deep pockets that accommodate the bulky aromatic amino acid side chains and represent attractive targets for small molecules (19, 20, 24). These conformational changes nevertheless also make it difficult to rationally design drugs that bind this protein interaction surface (25).

Author contributions: E.E.-P., A.A.A., J.D.B., R.K.G., P.W., and R.J.F. designed research; E.E.-P., A.A.A., P.N., E.D.R., E.M., and P.W. performed research; E.E.-P., A.A.A., P.N., E.D.R., R.B., P.P., K.M.S., R.K.G., and P.W. contributed new reagents/analytic tools; E.E.-P., A.A.A., P.N., J.D.B., R.K.G., P.W., and R.J.F. analyzed data; and E.E.-P., A.A.A., J.D.B., R.K.G., P.W., and R.J.F. wrote the paper.

Conflict of interest statement: J.D.B. has proprietary interests in and serves as a consultant to Karo Bio AB, which has commercial interests in the nuclear receptor field.

Freely available online through the PNAS open access option.

Abbreviations: AF-2, activation function 2; AR, androgen receptor; BF, binding function; DHT, dihydrotestosterone; FLF, flufenamic acid; FP, fluorescence polarization; K10, 1-*tert*-butyl-3-(2,5-dimethyl-benzyl)-1H-pyrazolo[3,4-D]pyrimidin-4-ylamine; LBD, ligand-binding domain; 2MI, 2-methylindole; NR, nuclear receptor; RB1, 3-((1-tert-butyl-4-amino-1H-pyrazolo[3,4-D]pyrimidin-3-yl)methyl)phenol; SRC, steroid receptor coactivator; TOL, tolfenamic acid; Triac, 3,3′,5-triiodothyroacetic acid; T_3, triiodothyronine; UCSF, University of California, San Francisco.

Data deposition: The atomic coordinates and structure factors have been deposited in the Protein Data Bank, www.pdb.org (PDB ID codes 2PIO, 2PIP, 2PIQ, 2PIR, 2PIT, 2PIU, 2PIV, 2PIW, 2PIX, 2PKL, and 2QPY).

‖To whom correspondence may be addressed. E-mail: jbaxter918@aol.com or flett@cgl.ucsf.edu.

This article contains supporting information online at www.pnas.org/cgi/content/full/0708036104/DC1.

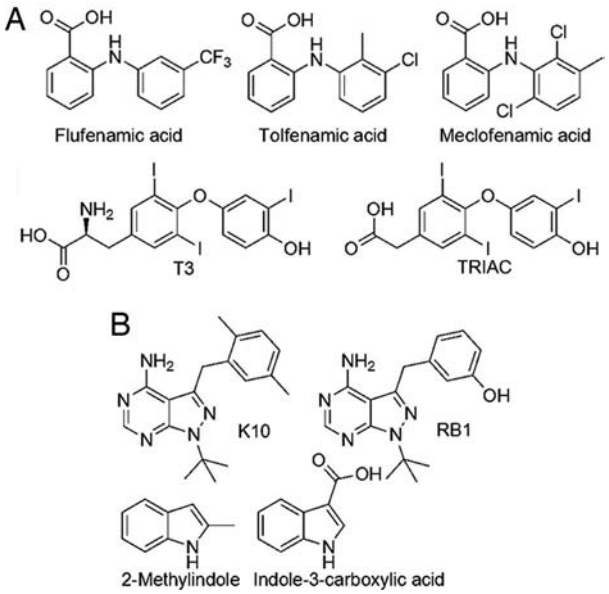

Fig. 1. Small molecules that bind AR. (*A*) Compounds exceeding 40% inhibition of AR LBD/SRC2–3 interaction along with T_3. FLF, Triac, and T_3 were also identified by x-ray screen. (*B*) Compounds uniquely identified by x-ray screen.

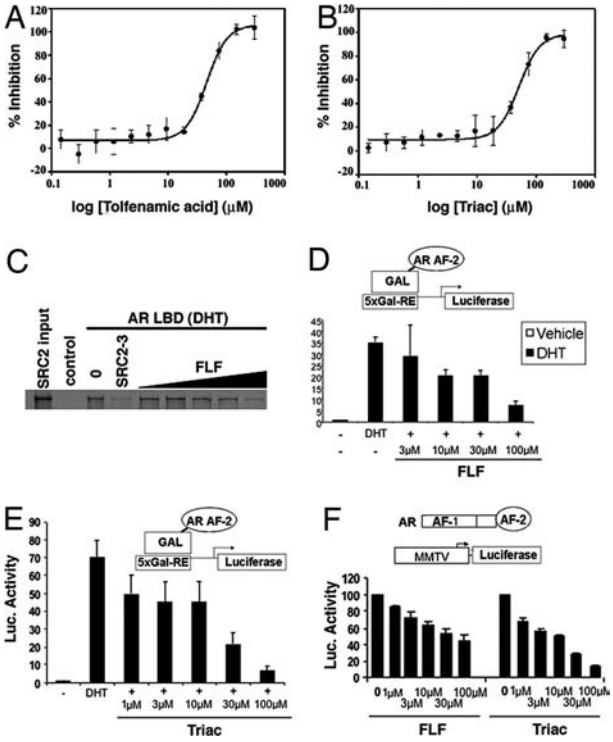

Fig. 2. Inhibition of coregulator binding and AR AF-2 activity. (*A* and *B*) FP dose–response analysis of TOL (*A*) and Triac (*B*) with AR LBD and SRC2–3. (*C*) SDS/PAGE of *in vitro* translated SRC2 retained in pull-downs with AR LBD/DHT complex plus vehicle (0) and 10 μg of SRC2–3 peptide or FLF (1, 3, 10, 30, and 100 μM). (*D* and *E*) AF-2 activity. Components are shown in a schematic at the top. Graphs show luciferase assays (light units $\times 10^4$) normalized to β-galactosidase. Standard errors were derived from sextuplet points. Similar results were obtained more than five times. (*F*) AR activity. Components are shown in a schematic at the top. Data represent a typical experiment with DHT response = 100%.

In the current study we identified several AR surface-interacting compounds that inhibit AR AF-2 activity with complementary functional and structural screens. Similar strategies were successful for drug development in other settings (25–28) and were instrumental in development of a drug that works at the protein product of the murine double minute gene (mdm2), a negative regulator of p53 tumor suppressor (29). We find, unexpectedly, that the most potent compounds bind preferentially to a novel site, BF-3, which allosterically influences coregulator association with AF-2, represents a new target for modulation of AR activity, and may be a previously unknown AR regulatory surface. Our results emphasize the potential of x-ray crystallography for detection of regulatory sites on NR surfaces.

Results

Solution Screening Detects Inhibitors of AR/SRC2 Interactions. We used automated fluorescence polarization (FP) (14) to screen for compounds that bind AR and inhibit coregulator association. This assay detects binding of AR AF-2 to a 15-aa LXXLL peptide overlapping the third SRC2 NR box (SRC2–3) in the presence of the androgen dihydrotestosterone (DHT); SRC2–3 binds with an apparent equilibrium dissociation constant (K_d) of 2.2 μM and is the tightest AR binding peptide in a library of LXXLL and FXXLF motifs (20). More than 55,000 compounds were screened. Most were from the Bay Area Screening Center library (ChemDiv/ChemBridge), comprising relatively large compounds (>400 Da) selected for diversity, solubility, and lack of toxicity. Also included was the collection of ≈1,200 off-patent drugs from Prestwick (Illkirch, France).

We detected four compounds that inhibited AR interactions with SRC2–3 by 40% or more at a concentration of 50 μM (Fig. 1*A*), all from the Prestwick library. These were three nonsteroidal antiinflammatory drugs, flufenamic acid (FLF), tolfenamic acid (TOL), and meclofenamic acid, (30), and 3,3′,5-triiodothyroacetic acid (Triac), a low-abundance thyroid hormone (31). These compounds share several features, including methylene or amine bridged phenyl rings and the carboxylic acid group. Each inhibited AR interactions with SRC2–3 in a dose-dependent fashion [Fig. 2 *A* and *B* and supporting information (SI) Table 1], with TOL showing the highest potency (IC_{50} = 47 μM). Competition isotherms exhibited saturation at high concentrations, implying the presence of defined binding sites on the AR LBD and that effects are not caused by nonspecific denaturation of AR protein. We later determined that the common active thyroid hormone triiodothyronine (T_3) (31) also inhibits AR/SRC2–3 interactions by ≈24% at 50 μM (data not shown). The fact that only five of 55,000 compounds inhibited AR interactions with SRC2–3 is indicative of high specificity in the assay.

Inhibition of AR Activity. FLF blocked AR LBD binding to a full-length coactivator. Similar to FP assays, FLF inhibition of AR LBD interactions with radiolabeled SRC2 *in vitro* was detected with 10–50 μM FLF, and 100 μM FLF inhibited SRC2 binding as efficiently as excess unlabeled SRC2–3 competitor peptide (Fig. 2*C*). Triac activity could not be evaluated in these assays; it caused AR LBD to precipitate in pull-downs.

All four compounds inhibited AR activity in cultured cells. FLF (Fig. 2*D*) and Triac (Fig. 2*E*) inhibited DHT response with AR LBD tethered to a reporter with a GAL DNA binding function and full-length AR active at the mouse mammary tumor virus (MMTV) promoter (Fig. 2*F*). Effects were dose-dependent with inhibition at 10–30 μM FLF. Similar results were obtained with TOL and meclofenamic acid (data not shown) and in several cell types (data not shown). The nonsteroidal antiinflammatory drugs and Triac did not inhibit GAL fusions linked

BIOCHEMISTRY

to activation domains from VP16 and CBP, confirming that effects are not related to toxicity (data not shown).

X-Ray Screens Reveal AR-Interacting Molecules at AF-2 and a New Site (BF-3). We also performed structural screens for AR-interacting compounds (32). AR LBD-DHT crystals were soaked with individual chemicals in groups of 1–10, and interacting compounds were localized by x-ray diffraction and visual inspection of electron densities (SI Table 2). Soaks were performed with the Prestwick library mentioned above and two libraries of chemical fragments that are unlikely to bind the AR with high affinity but were nonetheless chosen for their potential to be linked or modified to create tighter binding scaffolds. One library, assembled at the University of California, San Francisco (UCSF), comprises 400 protein kinase inhibitors and related compounds with characteristics of heterocyclic rings, similar to side chains of FXXLF motifs. The second is a proprietary library of 200 chemicals with multiple functionalities (BioBlocks).

We found seven drugs at the AR surface. From the Prestwick library we detected FLF, Triac, and T_3 (also identified in solution screens). We could not assess TOL and meclofenamic acid binding because these compounds disrupt AR crystals and it was possible to obtain FLF data sets only with short soaks (15 min). We also detected four compounds from the UCSF library (Fig. 1*B*). 1-*tert*-butyl-3-(2,5-dimethyl-benzyl)-1H-pyrazolo[3,4-D]pyrimidin-4-ylamine (K10) and 3-((1-tert-butyl-4-amino-1H-pyrazolo[3,4-D]pyrimidin-3-yl)methyl)phenol (RB1) are kinase inhibitors with two aromatic rings; 2-methylindole (2MI) and indole acetic acid resemble tryptophan indole rings. None of the UCSF library compounds promotes SRC2–3 dissociation in FP assays (data not shown), as expected from library design of probable low-affinity binders.

Unexpectedly, the compounds that displace SRC2–3 from AF-2, FLF, Triac, T_3, and two low-affinity compounds, 2MI and indole-3-carboxylic acid, bind to a previously unknown site, BF-3 (Fig. 3). This is a hydrophobic cleft at the junction of H1, the H3–H5 loop, and H9 that is almost as large as AF-2 and exhibits characteristics of protein interaction surfaces (developed below).

None of the compounds appear at AF-2 in short soaks, but Triac, T_3, 2MI, and kinase inhibitors K10 and RB1 eventually appeared at this location with soaks of 7–20 h. FLF damages AR crystals at these times. Slow appearance of small molecules at AR AF-2 is not related to inaccessibility; crystal soaks with SRC2–3 peptide revealed electron density corresponding to the LxxLL motif at AF-2 within 1 h (data not shown).

Together, the studies confirm that it is feasible to detect AR surface-interacting compounds with x-ray screens, that small molecules bind AF-2, and, surprisingly, a novel small molecule binding site, BF-3.

AR Surface-Interacting Compounds Bind Preferentially to BF-3. X-ray structures suggest that Triac interacts preferentially at BF-3 vs. AF-2 (Fig. 4 and SI Table 3). Triac covers 580 Å^2 of both surfaces yet exhibits stronger, uniformly well defined electron density at BF-3; the Triac proximal and distal phenyl rings make hydrophobic contacts with a large BF-3 surface comprising Pro-723, Phe-673, and Ile-672 from H1, Gly-724 and Asn-727 from H3–5, and Phe-826, Glu-829, Glu-837, Arg-840, and Asn-833 from H9 (Fig. 4 *A* and *C*). In addition, the distal phenyl ring hydroxyl group hydrogen-bonds with Asn-727, and the proximal phenyl ring carboxylate hydrogen-bonds with the oppositely charged Arg-840 side chain. Weaker association at AF-2 is due to poor fit (Fig. 4 *D* and *F*). The Triac distal ring is well defined and makes hydrophobic contacts with a deep AF-2 subpocket (S1) that hosts F_1 or L_1 of the signature motif $F_1XXL_4F_5/L_1XXL_4L_5$, but the proximal phenyl ring is poorly defined and spans the S2 and S3 subsites that host L_4 and F_5/L_5 (Fig. 4*D*). T_3 displayed similar binding modes to Triac at both sites (data not shown).

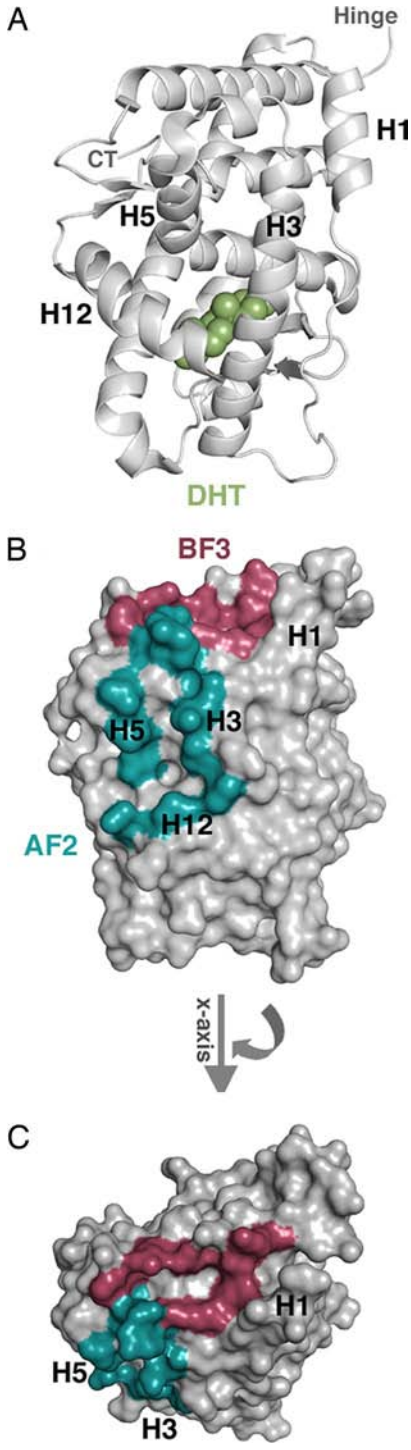

Fig. 3. AF-2 and BF-3. (*A*) Schematic of AR LBD showing location of DHT, key AF-2 helices 3, 5, and 12, and H1. (*B*) Space-filling model showing residues in AF-2 (cyan) and BF-3 (red). (*C*) As in *B*, rotated 90° to reveal BF-3.

Interactions at BF-3 are well defined for other compounds. FLF aromatic rings interact tangentially with BF-3 to bury 520 Å^2 of solvent-exposed surface (Fig. 4 *B* and *C*). Whereas 2MI displays a binding mode similar to the Triac distal phenyl ring and buries, respectively, 280 Å^2 and 370 Å^2 of accessible BF-3 and AF-2 surfaces, it is better resolved at BF-3 (data not shown). Indole-3-carboxylic acid binds BF-3 in a similar mode to 2MI and also appears well defined (data not shown). By contrast, K10 and

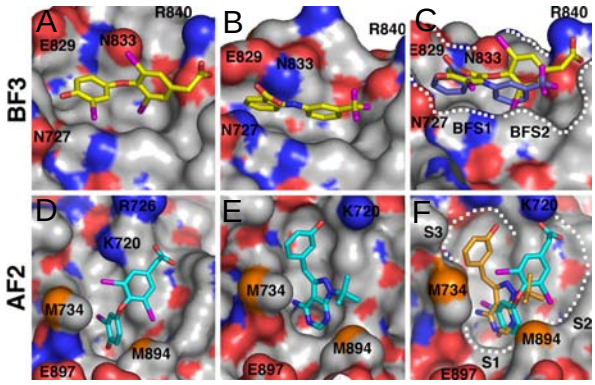

Fig. 4. Interactions at the AR LBD surface. (*A–C*). BF-3 including Glu-829, Asn-833, Arg-840, Phe-673, and Tyr-834 is highlighted by dots and divided into two subpockets that accommodate Triac and FLF phenolic rings. Basic residues are in blue, and acidic residues are in red. Shown are close-ups of interactions with Triac (*A*) and FLF (*B*) as yellow stick models. (*C*) Superimposed Triac (yellow) plus FLF (dark blue). (*D–F*) AF-2 lined by Met-734, Lys-720, Glu-897, and Met-894 with subsites (S1–S3) highlighted by dots. Basic residues are in blue, acidic residues are in red, and Met is in yellow. *D* and *E* show close-ups of Triac and RB1, respectively. (*F*) Superimposed Triac (blue) plus RB1 (orange). Triac interacts with S1 and the area between S2 and S3 whereas RB1 interacts with S1 and S3.

RB1 occupy ≈580 Å^2 of solvent-exposed AF-2 surface but exhibit even weaker electron density than Triac (Fig. 4 *E* and *F* and data not shown). Both compounds engage in hydrophobic interactions with S1 and S3, with better definition at S1 (Fig. 4*F*).

Interactions at BF-3 Weaken Coactivator Binding. Comparison of the AR surface with or without Triac, T_3, and FLF reveals structural alterations. Four BF-3 residues (Arg-840, Asn-727, Phe-826, and Glu-829) that point out of the pocket into solution point inward and engage the compound (Fig. 5*A*). This is accompanied by large movements of the Arg-726 side chain, close to AF-2, and repositioning of AF-2 residues Lys-717 and Met-734 (data not shown). There are also small but significant shifts in secondary structural elements; residues 720–730 (H3) and 825–847 (H9) exhibit rmsd of 0.33 and 0.44, respectively. Thus, Triac and FLF promote structural rearrangements in BF-3 that are propagated to AF-2.

Drug interactions at BF-3 cause coregulator peptides that are bound to AF-2 to become disordered. In crystals of ternary complexes of AR LBD-DHT-SRC2–3 (LXXLL) and AR LBD-DHT-ARA70 (FXXLF), the peptides fold into α-helices of 15 and 9 amino acids (20), respectively, clearly defined by electron density (Fig. 5 *A Right* and *B Right*). Short Triac incubations result in loss of electron density in the regions that flank SRC2–3 hydrophobic triads (Fig. 5*A*) and disruption of Arg-726 interactions with SRC2–3 residues that lie C-terminal to the LxxLL motif. Triac binding to BF-3 also weakened ARA70 FxxLF contacts (Fig. 5*B*); only four residues are visible with Leu+4 and Phe+5 completely defined (Fig. 5*B Right*). Arg-726 does not contact the FXXLF peptide, suggesting that reorganization of AF-2 itself is important for this effect. Unexpectedly, Arg-840 adopts the inward-facing conformation in this experiment (Fig. 5*B*). Similar Arg-840 rearrangements are also seen with artificial FXXLF peptides (19), suggesting that it is a hitherto unappreciated feature of AR interactions with these NR boxes. It is unlikely that Triac interacts directly with AF-2 to disrupt coactivator binding, because it is not detected at AF-2 at these times and the electron-rich iodine groups of Triac represent particularly good markers. Control soaks with solvent (DMSO) reveal no similar effects on coregulator peptide organization (data not shown). Thus, Triac interactions at BF-3 weaken contacts between AR and coactivator peptides.

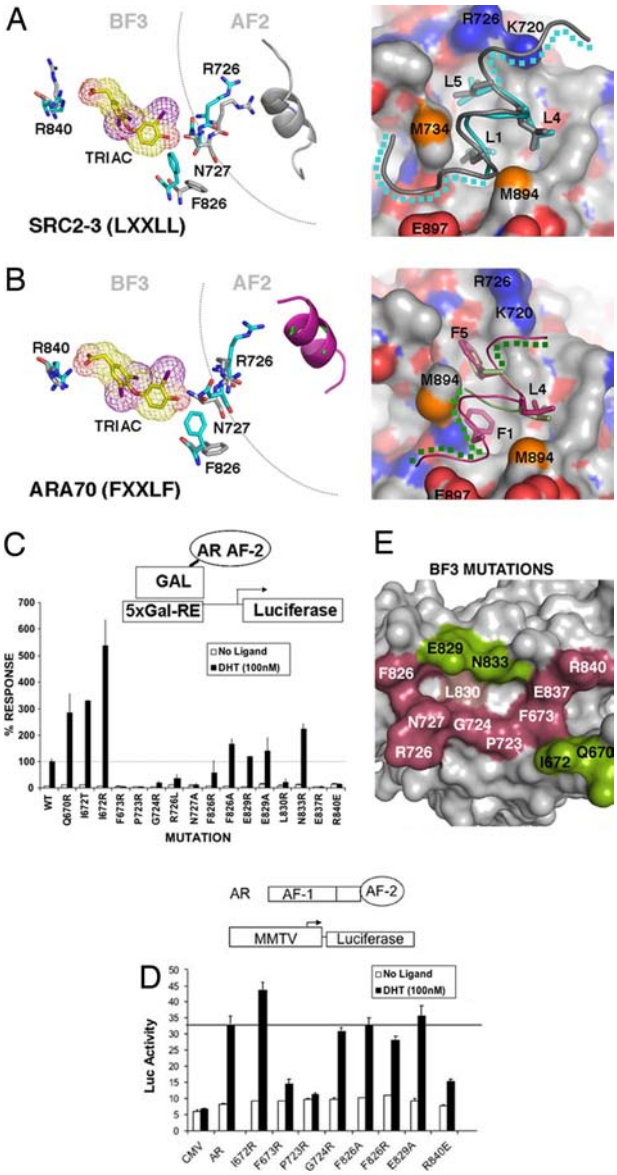

Fig. 5. BF-3 modulates AF-2. (*A*) Superposition of AR with SRC2–3 with Triac (blue sticks), without Triac (gray sticks), and with Triac with no peptide (yellow sticks). Arg-840, Phe-826, Asn-727 (BF-3), and Arg-726 (AF-2) adopt different conformations. Without Triac, Arg-840 points outward and Arg-726 contacts SRC2–3 (gray). With Triac, Arg-840 contacts ligand and Arg-726 does not contact SRC2–3 (blue). (*Right*) SRC2–3 without Triac (gray trace) and with Triac (blue trace). Blue dots indicate regions not visible with Triac; Leu residues are shown as sticks. (*B*) As in *A*, with ARA70 with Triac (blue) and without Triac (gray). Reorganization is similar to *A* except that Arg-840 points inward without Triac. (*C*) AR AF-2 assay; wild type = 100%. Results are averages of at least three different experiments. (*D*) Transfection with full-length AR active at MMTV-Luc. (*E*) BF-3 defined by mutagenesis. Raspberry, residues needed for activity; green, mutations that increase activity.

If BF-3 is important for AR action, then BF-3 mutations should alter AR activity. Mutations at Gln-670, Ile-672, and Leu-830 are associated with prostate cancer (33–35). Leu-830, Pro-723, Gly-724, and Arg-840 are mutated in androgen insensitivity syndrome (36) (www.androgendb.mcgill.ca). Targeted mutagenesis of Asn-727 and Arg-840, which move on Triac binding, eliminate AR LBD activity (Fig. 5*C*), similar to inhi-

bition obtained with mutations in AF-2 (20). Likewise, mutations at Phe-673, Pro-723, Glu-724, Glu-737, and, possibly, Arg-726 and Phe-826 reduce activity. Mutations in nearby residues, Gln-670, Ile-672, Glu-829, and Asn-833, increase AR AF-2 activity up to 5-fold. Similar results were obtained with full-length AR at MMTV-LUC; mutations at Phe-673, Pro-723, and Arg-840 inhibited androgen response (Fig. 5*D*). The mutations that inhibit AR activity describe a continuous patch that resembles the BF-3 surface defined by chemical interactions (Fig. 5*E*).

BF-3 could be present in other NRs. Part of the site, the H3–H4 loop, is a signature sequence (37). Superposition of published structures reveals conservation of BF-3 residues in the steroid subfamily (SI Fig. 6). Mutations in equivalent regions of estrogen and glucocorticoid receptor are implicated in coactivator binding (38, 39). Collectively, these data provide evidence for a role of BF-3 in NR action.

Discussion

We used two screens to identify molecules that inhibit AR activity by binding the AR LBD surface at important sites. FP screening detects four drugs that inhibit SRC2–3 peptide binding with $IC_{50} \approx 50$ μM in a library of 55,000 compounds (FLF, TOL, meclofenamic acid, and Triac). T_3 was identified on the basis of its similarities to Triac. X-ray screening of three small compound libraries (Prestwick, UCSF kinase inhibitors, and BioBlocks) detected seven compounds, including three that were identified in functional screens (FLF, Triac, and T_3) and new compounds (RB1, K10, 2MI, and indole-3-carboxylic acid).

Our most surprising finding is that the best inhibitors interact preferentially with a novel surface site (BF-3). Three lines of evidence suggest that ligand interactions with BF-3 exert indirect effects on AF-2 to inhibit coregulator binding. First, FLF and Triac promote reorganization of BF-3 residues (Asn-727, Phe-826, Glu-829, and Arg-840) and AF-2 residues (Met-734 and Lys-717) and large-scale repositioning of Arg-726 at the AF-2 boundary. Second, short Triac soaks weaken AR interactions with FXXLF and LXXLL peptides in AR-DHT-NR box crystals. Third, BF-3 residues are required for optimal AR AF-2 activity in cell culture. We considered the possibility that compounds displace SRC2–3 through weak interactions with AF-2. In this case, rapid binding of compounds to BF-3 may reflect crystal packing constraints that render BF-3 available for drug interactions. We believe that this is unlikely because a bulky SRC2–3 peptide appears rapidly at AR AF-2 in crystal soaks (data not shown), but we cannot yet rule out this possibility. The models are not mutually exclusive; BF-3-dependent effects could complement weak binding of compounds to AF-2.

The natural role of BF-3 *in vivo* is unknown, but our data, coupled with natural mutations, suggest that the site is important. Mutations at Gln-670, Ile-672, and Leu-830 enhance AR action in prostate cancer (33, 35, 40), and mutations at Gln-670 and Ile-672 enhance AR AF-2 activity (Fig. 5*C*). BF-3 is a target for androgen insensitivity syndrome mutations at Ile-672, Leu-830, Arg-840, and Asn-727, with mutations in the latter two diminishing SRC2 binding *in vitro* although neither contacts coregulator (41). Finally, mutations in BF-3 of other NRs are implicated in coactivator binding (38, 42). BF-3 could bind regulatory proteins or other AR domains and could, for example, communicate information about DNA binding domain position to the LBD and AF-2 and vice versa.

Regardless of the mechanism by which compounds displace SRC2–3, the fact that we detect such compounds for ARs and TRs (14) suggests that functional and structural screens are viable methods for NR inhibitor development. High-throughput functional screens detect inhibitors among large libraries of drug-like compounds, and our experience with ARs and TRs suggests that "hits" are uncommon but are specific and rarely false positives. It is not feasible to perform high-throughput x-ray screens with large libraries, but this method complements functional screens in three ways. First, x-ray screens provide information about binding of leads. For example, Triac, RB1, and K10 interact preferentially with AF-2 S1, so strategies to improve binding to S2 or S3 would yield higher-affinity compounds. Second, x-ray screening reveals unexpected sites or interaction modes; the discovery of BF-3 was a surprise. Third, x-ray screens are the only known method to identify weakly interacting compounds that bind the surface with high ligand efficiency and comprise building blocks for tight binding compounds.

It may be feasible to develop three types of small molecules that modulate AR and NR activity: classical drugs that bind BF-1, drugs that bind surface-exposed active sites such as AF-2, or drugs that bind surface allosteric sites such as BF-3. This greatly expands the number of NR pharmaceutical targets and the potential spectrum of responses, and representatives of each class could even be used together. The fact that three leads are off-patent aspirin derivatives approved for human use (30), and that others are thyroid hormones with known actions in humans, raises the possibility that such compounds could be used for prostate cancer treatment. It is unlikely that natural T_3 or Triac concentrations approach levels required to bind the AR surface *in vivo* (31), but it is intriguing to speculate that AR surface interactions contribute to documented inhibitory effects of nonsteroidal antiinflammatory drugs on growth and survival of prostate cancer cells (43). We propose that well designed compounds engaging AF-2 or BF-3 will modulate coregulator recruitment in physiological settings, including cancer, and that combined functional/x-ray screening is a useful strategy for identification of ligands that act at NR surfaces.

Materials and Methods

Peptide Synthesis. Five milligrams of SRC2–3 (CKENALLRYLLDKDD) was dissolved in 1 ml of PBS and added to 50 mg of 5-iodoacetamidofluorescein in 1 ml of DMF. After 3 h at room temperature, 0.5 ml of ethanethiol was added and peptide was purified by HPLC [XTerra C18 column: A, water (0.05% TFA); B, CH3CN (0.05% TFA), linear gradient 0100% over 25 min; Waters]. Evaporation of fractions gave 3.8 mg of labeled peptide. Mass analysis (MALDI-TOF) showed one species at 2,195.8 (*m/z*).

Protein Expression. AR LBD (residues 663–919) was expressed in *Escherichia coli* in the presence of DHT and purified by using published protocols (20). Functionality was determined by SRC2–3 binding in FP assays (20); K_d for SRC2–3 binding was 2.7 μM.

Solution Screening. Plates (384 wells; Costar 3710) were prepared with 4 μl of compound (5 mM in DMSO) plus 80 μl of dilution buffer (20 mM Tris·HCl/100 mM NaCl, pH 7.2/1 mM DTT/1 mM EDTA/0.01% Nonidet P-40/10% glycerol/10.5% DMSO) by using a WellMate (Matrix). Five microliters from the dilution plates was transferred to 384-well assay plates followed by 20 μl of protein mixture (6.25 μM AR plus DHT and 0.0125 μM peptide in dilution buffer; final concentration 50 μM compound, 4% DMSO). FP was measured after 2 h (excitation λ 485 nm, emission λ 530 nm) on an AD plate reader (Molecular Devices). Longer incubation times led to inhibition of FP in negative controls (DMSO only), possibly reflecting AR instability. For dose–response, compounds were diluted from 5,000 to 2.44 μM in DMSO into a 96-well plate (Costar 3365). Twenty microliters of mixture was added to 1.2 μl of compounds in 384-well plates (Costar 3710), yielding a final concentration of 300 to 0.146 μM, and equilibrated for 5 h before FP. Data were analyzed by using SigmaPlot 8.0 (SPSS, Chicago, IL), and K_d values were obtained by fitting data to y = minimum + (maximum − minimum)/1 + (x/K_d) Hill slope.

Library Assembly for X-Ray Screens. Three libraries with different characteristics were used. A commercial library of 1,120 FDA-approved drugs was from Prestwick. Compounds with protein kinase inhibitor characteristics or multiple heterocyclic rings were from UCSF. Two hundred small compounds <200 Da with druglike character, designed as building blocks for larger molecules, were from BioBlocks.

X-Ray Screening. Compounds were dissolved in DMSO at 10–20 mM and soaked with AR:DHT crystals on 96-well plates. Typically, a drop with one to four AR crystals is soaked with 1–10 compounds. Increasing 0.2 μl units of compound are added, and crystals are monitored. If crystals survive, another 0.2 μl is added until crystals show fatigue. Fresh crystals plus maximum tolerated chemical volume were used for cryo treatment and freezing.

Crystallization, Structure Determination, and Refinement. Approximately 80 crystals were flash-cooled in liquid N_2 for analysis at the Lawrence Berkeley National Laboratory Advanced Light Source (beamline 8.3.1) in each trip. Only data sets from crystals that diffract <2.5 Å were collected. All compounds that cause AR LBD crystals to diffract poorly were checked afterward, and soaks with lower concentration were performed. Data sets from 35 crystals were measured per 8-h shift and indexed and merged by using ELVES. Molecular replacement solutions were obtained by using rotation and translation functions from CNS software. Model building used QUANTA (Accelrys Software) monitored by using free *R* factor. Visual inspection of electron densities using QUANTA allows identification of interacting compounds. A composite omit map was also calculated absent 5% of the molecule to remove model bias. Calculation of electron density and crystallographic refinement was performed with CNS by using target parameters of Engh and Huber. Several cycles of model building, conjugate gradient minimization, and simulated annealing resulted in structures with good stereochemistry. A Ramachandran plot shows that most residues fall into favored regions (SI Table 2).

Pull-Downs and Transfections. Vectors, expression and labeling, and assay procedures were previously described (20). New mutants were made by QuikChange Site-Directed Mutagenesis (Stratagene).

We thank Pascal Egea, Elena Sablin, Anang Shelat, and Arnold T. Hagler for discussions; James Holton and George Meigs for assistance at the Advanced Light Source (beamline 8.3.1); and Chao Zhang (UCSF) for K10. This work was supported by the Prostate Cancer Foundation (R.J.F. and P.W.); National Institutes of Health Grants DK58080 (to R.J.F. and R.K.G.), DK41482 (to J.D.B.), and DK51281 (to J.D.B.); Specialized Programs of Research Excellence/National Cancer Institute Grant CA89520 (to E.E.-P.); Department of Defense Grants W81XWH-05-1-0545 (to R.J.F.) and PC030607 (to P.W.); the UCSF Prostate Cancer Program (P.W.); and a Herbert Boyer Postdoctoral Fellowship (to E.E.-P.).

1. Laudet V, Gronemeyer H (2002) *The Nuclear Receptor Facts Book* (Academic, London).
2. Baxter JD, Goede P, Apriletti JW, West BL, Feng W, Mellstrom K, Fletterick RJ, Wagner RL, Kushner PJ, Ribeiro RC, *et al.* (2002) *Endocrinology* 143:517–524.
3. Weatherman RV, Fletterick RJ, Scanlan TS (1999) *Annu Rev Biochem* 68:559–581.
4. Nettles KW, Greene GL (2005) *Annu Rev Physiol* 67:309–333.
5. Rosenfeld MG, Lunyak VV, Glass CK (2006) *Genes Dev* 20:1405–1428.
6. Lonard DM, O'Malley BW (2006) *Cell* 125:411–414.
7. Borngraeber S, Budny MJ, Chiellini G, Cunha-Lima ST, Togashi M, Webb P, Baxter JD, Scanlan TS, Fletterick RJ (2003) *Proc Natl Acad Sci USA* 100:15358–15363.
8. Mitro N, Mak PA, Vargas L, Godio C, Hampton E, Molteni V, Kreusch A, Saez E (2007) *Nature* 445:219–223.
9. Dehm SM, Tindall DJ (2006) *J Cell Biochem* 99:333–344.
10. Lewis-Wambi JS, Jordan VC (2005) *Breast Dis* 24:93–105.
11. Scher HI, Sawyers CL (2005) *J Clin Oncol* 23:8253–8261.
12. Darimont BD (2003) *Chem Biol* 10:675–676.
13. Feng W, Ribeiro RC, Wagner RL, Nguyen H, Apriletti JW, Fletterick RJ, Baxter JD, Kushner PJ, West BL (1998) *Science* 280:1747–1749.
14. Arnold LA, Estebanez-Perpina E, Togashi M, Jouravel N, Shelat A, McReynolds AC, Mar E, Nguyen P, Baxter JD, Fletterick RJ, *et al.* (2005) *J Biol Chem* 280:43048–43055.
15. Arnold LA, Estebanez-Perpina E, Togashi M, Shelat A, Ocasio CA, McReynolds AC, Nguyen P, Baxter JD, Fletterick RJ, Webb P, Guy RK (2006) *Sci STKE* 2006:pl3.
16. Wang Y, Chirgadze NY, Briggs SL, Khan S, Jensen EV, Burris TP (2006) *Proc Natl Acad Sci USA* 103:9908–9911.
17. Rodriguez AL, Tamrazi A, Collins ML, Katzenellenbogen JA (2004) *J Med Chem* 47:600–611.
18. Chang CY, Abdo J, Hartney T, McDonnell DP (2005) *Mol Endocrinol* 19:2478–2490.
19. Hur E, Pfaff SJ, Payne ES, Gron H, Buehrer BM, Fletterick RJ (2004) *PLoS Biol* 2:E274.
20. Estebanez-Perpina E, Moore JM, Mar E, Delgado-Rodrigues E, Nguyen P, Baxter JD, Buehrer BM, Webb P, Fletterick RJ, Guy RK (2005) *J Biol Chem* 280:8060–8068.
21. Chang CY, McDonnell DP (2005) *Trends Pharmacol Sci* 26:225–228.
22. Heinlein CA, Chang C (2004) *Endocr Rev* 25:276–308.
23. He B, Wilson EM (2002) *Mol Genet Metab* 75:293–298.
24. He B, Gampe RT, Jr, Kole AJ, Hnat AT, Stanley TB, An G, Stewart EL, Kalman RI, Minges JT, Wilson EM (2004) *Mol Cell* 16:425–438.
25. Wells J, Arkin M, Braisted A, DeLano W, McDowell B, Oslob J, Raimundo B, Randal M (2003) *Ernst Schering Res Found Workshop* 19–27.
26. Arkin MR, Wells JA (2004) *Nat Rev Drug Discovery* 3:301–317.
27. Berg T (2003) *Angew Chem Int Ed Engl* 42:2462–2481.
28. Toogood PL (2002) *Curr Opin Chem Biol* 6:472–478.
29. Vassilev LT, Vu BT, Graves B, Carvajal D, Podlaski F, Filipovic Z, Kong N, Kammlott U, Lukacs C, Klein C, *et al.* (2004) *Science* 303:844–848.
30. Flower R (2003) *Nat Rev Drug Discovery* 2:179–191.
31. Braverman LE, Utiger RD (2000) (Lippincott Williams & Wilkins, Philadelphia).
32. Nienaber VL, Richardson PL, Klinghofer V, Bouska JJ, Giranda VL, Greer J (2000) *Nature* 18:1105–1108.
33. Buchanan G, Yang M, Harris JM, Nahm HS, Han G, Moore N, Bentel JM, Matusik RJ, Horsfall DJ, Marshall VR, *et al.* (2001) *Mol Endocrinol* 15:46–56.
34. Buchanan G, Greenberg NM, Scher HI, Harris JM, Marshall VR, Tilley WD (2001) *Clin Cancer Res* 7:1273–1281.
35. Shi XB, Ma AH, Xia L, Kung HJ, de Vere White RW (2002) *Cancer Res* 62:1496–1502.
36. McPhaul MJ (2002) *Mol Cell Endocrinol* 198:61–67.
37. Brelivet Y, Kammerer S, Rochel N, Poch O, Moras D (2004) *EMBO Rep* 5:423–429.
38. Tanenbaum DM, Wang Y, Williams SP, Sigler PB (1998) *Proc Natl Acad Sci USA* 95:5998–6003.
39. Milhon J, Lee S, Kohli K, Chen D, Hong H, Stallcup MR (1997) *Mol Endocrinol* 11:1795–1805.
40. Chavez B, Vilchis F, Zenteno JC, Larrea F, Kofman-Alfaro S (2001) *Clin Genet* 59:185–188.
41. Lim J, Ghadessy FJ, Abdullah AA, Pinsky L, Trifiro M, Yong EL (2000) *Mol Endocrinol* 14:1187–1197.
42. Milhon J, Lee S, Kohli K, Chen D, Hong H, Stallcup MR (1997) *Mol Endocrinol* 11:1795–1805.
43. Andrews P, Krygier S, Djakiew D (2002) *Cancer Chemother Pharmacol* 49:179–186.

Molecular Endocrinology. First published ahead of print September 6, 2007 as doi:10.1210/me.2007-0174

Structural Insight into the Mode of Action of a Direct Inhibitor of Coregulator Binding to the Thyroid Hormone Receptor

Abbreviated Title: Inhibitor of TRβ Coregulator Binding

Eva Estébanez-Perpiñá[a,*], Leggy A. Arnold[b,*], Natalia Jouravel[a,*], Marie Togashi[c], Justin Blethrow[d], Ellena Mar[a], Phuong Nguyen[c], Kevin J. Phillips[c], John D. Baxter[c], Paul Webb[c], R. Kiplin Guy[b], and Robert J. Fletterick[a]

[a]Dept. Biochemistry & Biophysics, University California San Francisco (UCSF), 600 16th Street, Genentech Hall, San Francisco, CA 94158, USA. Tel: 415-476-5051; Fax: 415-476-1902; email: eva@msg.ucsf.edu / njouravel@msg.ucsf.edu / emar@msg.ucsf.edu / flett@msg.ucsf.edu
[b]Dept. Chemical Biology & Therapeutics, St Jude Children's Research Hospital, 332 North Lauderdale, Memphis, TN 38105, USA. Tel: 901-495-5714; Fax: 901-495-5715; email: Alexander.Arnold@STJUDE.ORG / Kip.Guy@STJUDE.ORG
[c]Diabetes Center & Dept. of Medicine, University California San Francisco (UCSF), 513 Parnassus Avenue, S-1222, Box 0540, Medical Sciences Building, San Francisco, CA 94143, USA. Tel: 415-476-6789; Fax: 415-564-5813; email: mtogashi@diabetes.ucsf.edu / pnguyen@diabetes.ucsf.edu / JBaxter918@aol.com / pwebb@diabetes.ucsf.edu
[d]Dept. Cellular & Molecular Pharmacology, University California San Francisco (UCSF), 600 16th Street, Genentech Hall, San Francisco, CA 94143, USA. Tel: 415-514-0472; Fax: 415-514-0822; email: justin.blethrow@ucsf.edu

*Eva Estébanez-Perpiñá, Leggy A. Arnold, and Natalia Jouravel contributed equally to this work.

Address correspondence to: Robert J. Fletterick, Dept. Biochemistry & Biophysics, University of California, San Francisco CA 94158-2240, USA. Tel: 415-476-5051; Fax: 415-476-1902; email: flett@msg.ucsf.edu

Key words: thyroid receptor beta, nuclear hormone receptors, inhibitors, protein-protein interactions, coregulator binding, activation function 2 pocket, aromatic β-amino ketones, structure-based drug design, surface-interacting drugs

This work was supported in part by The Prostate Cancer Foundation and the American Lebanese Syrian Associated Charities (ALSAC) and by the NIH grants DK58080 (to RJF and RKG), DK41482, 61468, and 51281 (to JDB) and the SPORE NCI grant CA8952 and Herbert-Boyer Foundation (to EEP).

Disclosure Statement: JDB has proprietary interests in and serves as a consultant to Karo Bio AB (Huddinge, Sweden), which has commercial interests in this area of research. The other authors have nothing to disclose.

SUMMARY

The development of nuclear hormone receptor antagonists that directly inhibit the association of the receptor with its essential coactivators would allow useful manipulation of nuclear hormone receptor signalling. We previously identified 3-(dibutylamino)-1-(4-hexylphenyl)-propan-1-one (DHPPA), an aromatic β-amino ketone that inhibits coactivator recruitment to thyroid hormone receptor β (TRβ), in a high-throughput screen. Initial evidence suggested that the aromatic β-enone 1-(4-hexylphenyl)-prop-2-en-1-one (HPPE), which alkylates a specific cysteine residue on the TRβ surface, is liberated from DHPPA. Nevertheless, aspects of the mechanism and specificity of action of DHPPA remained unclear. Here, we report an X-ray structure of TRβ with the inhibitor HPPE at 2.3-Å resolution. Unreacted HPPE is located at the interface that normally mediates binding between TRβ and its coactivator. Several lines of evidence, including experiments with TRβ mutants and mass spectroscopic analysis, showed that HPPE specifically alkylates cysteine residue 298 of TRβ, which is located near the activation function-2 pocket. We propose that this covalent adduct formation proceeds through a two-step mechanism: first, β-elimination to form HPPE; second, a covalent bond slowly forms between HPPE and TRβ. DHPPA represents a novel class of potent TRβ antagonist, and its crystal structure suggests new ways to design antagonists that target the assembly of nuclear hormone receptor gene regulatory complexes and block transcription.

INTRODUCTION

The nuclear hormone receptor (NR) family of transcription factors is a target for pharmaceutical development, and many NR antagonists are in current use (1, 2). For example, estrogen receptor (ER) antagonists such as tamoxifen and faslodex inhibit growth and recurrence of estrogen-dependent breast cancer (3). Likewise, androgen receptor (AR) antagonists such as hydroxy-flutamide and bicalutamide are used to treat androgen-dependent prostate cancers (4, 5). Other available NR inhibitors include spironolactone, which reduces mortality after heart attack (6), and RU486, which is used as emergency birth control (7).

New NR inhibitors would most likely be useful for treating certain diseases. Thyroid hormone (TH) receptor (TR) antagonists could provide rapid-acting therapies for hyperthyroidism (excess TH production), particularly for use during thyroid storm, a life-threatening thyrotoxic crisis. Antagonists selective for the TRα isoform, which regulates heart rate, could be used to treat cardiac arrhythmias (8, 9).

NRs are composed of three modular domains (10, 11): the C-terminal ligand-binding domain (LBD), the ligand dependent transactivation function (AF-2), and the N-terminal transactivation function (AF-1) domain. Hormone binds the LBD and activates AF-2, which, in turn, recruits coactivators (12, 13). All NR antagonists that are currently available for clinical use competitively inhibit hormone binding (5). Most NR antagonists are believed to work either by precluding formation of an active LBD conformation or by inducing an aberrant LBD conformation that does not permit AF-2 activity. A number of alternate mechanisms have been suggested, including inhibition of NR via enhanced corepressor recruitment to a surface that partially overlaps AF-2, increased NR turnover, blockade of NR dimer formation, and inhibition of the AF-1 domain (13).

The molecular basis for NR antagonism is well understood (8, 9, 14). NR LBDs comprise a sandwich of three distinct layers formed by 11 to 12 α-helices (H1-H12) and four short β-strands with activating ligands enclosed in the hydrophobic core of the domain (15). Agonists enhance the packing of the C-terminal helix (H12) over the lower part of the LBD (H3 and H5), completing the AF-2 surface.(16) Many antagonists resemble cognate hormone but contain bulky extensions that displace H12. Others occupy the hormone-binding pocket but fail to form a hydrogen bond network, which is required for H12 packing (8). This knowledge has been already exploited to create new antagonists for TRs and many other NRs (8).

However, despite these successes, new NR antagonists are still needed. Many ligand-dependent NRs can influence transcription in the absence of hormone. For example, ERs and ARs acquire the capacity to activate transcription in the presence of antagonists during progression of breast or prostate cancer (17, 18). Furthermore, many NRs are not ligand dependent. The LBD of the orphan nuclear receptor Nurr1 lacks a conventional hormone-binding pocket, and ligands of the hepatocyte nuclear factor HNF-4α (14- to 18-chain fatty acids) bind tightly and are better described as prosthetic groups (19). We and others have suggested that directly blocking the coregulator-binding site would afford antagonists which have been referred to as surface-interacting drugs (SIDs). SIDs inhibit key NR protein-protein interaction surfaces and could block NR activity, irrespective of hormone responsiveness of the target cell or the presence or absence of the ligand (20-22). Additionally, SIDs that target unique regions of the NR surface should exhibit better specificity than conventional antagonists, which show troubling cross-reaction with hormone-binding pockets of closely related NRs.

The NR AF-2 surface is an attractive target for candidate SIDs, because it is deeply articulated and has significant hydrophobic character (15, 20, 23). Combined X-ray structural analysis and scanning-surface mutagenesis approaches indicated that TR AF-2 is a small concave surface and that only six hydrophobic residues (V284, K288, I302, K306, L454, and E457) are crucial for its function (24). This surface binds short coactivator domains (NR boxes) that conform to the consensus NR-

interaction motif LXXLL and form a short α-helices with one face being predominantly hydrophobic (24, 25).

In previous work, we identified two molecules that inhibit interactions between TRβ and the steroid receptor coactivator 2 (SRC2) with IC_{50} values of approximately 2 μM.(21) We also showed that one of these compounds, 3-(dibutylamino)-1-(4-hexylphenyl)-propan-1-one (DHPPA, Fig. 1) is more than 10-fold selective for TRβ over the closely related TRα isoform. DHPPA does not displace T_3 from TR *in vitro* but inhibits TRβ activity *in vivo* when the receptor is saturated with TH. It appears to have no gross effects upon protein structure or stability. Other groups have reported compounds that act on the ER (26-29).

Several lines of evidence suggested that DHPPA was a prodrug whose active species β-enone 1-(4-hexylphenyl)-prop-2-en-1-one (HPPE) acted irreversibly. DHPPA is a member of a class of compounds called Mannich bases, which undergo slow β-elimination in solution at physiological pH to form α,β-unsaturated ketones that alkylate nearby electron-rich groups, with a strong preference for nucleophilic sulphur such as that of cysteine side chains (30). We found that HPPE potently inhibits TRβ AF-2 activity in biochemical and cell culture models. Moreover, DHPPA inhibition of TRβ interactions with coactivators is time dependent and requires stoichiometric amounts of compound, hallmarks of irreversible inhibition. Finally, incubation of TRβ LBD with DHPPA increases TRβ molecular weight in a manner consistent with adduct formation between TRβ and a single HPPE molecule. We also noted that several cysteine residues are exposed on the TRβ surface, including three close to AF-2 (Cys309, Cys298, and Cys294). Mutation of Cys309 weakens the actions of DHPPA, though we did not confirm a covalent bond between this residue and HPPE.

In this study, we investigate the mechanism of DHPPA action by using X-ray crystallography and directed mutagenesis of the TRβ coactivator–binding surface. The results suggest that DHPPA inhibits TRβ action by rapidly liberating the reactiveα,β-unsaturated ketone HPPE at the TRβ AF-2 surface and that this intermediate, in turn, reacts in a slower step with the nearby Cys298 residue to occlude AF-2. This mechanism exploits the intrinsic activity of the SRC-binding site to generate intermediates that modify nucleophilic groups that are accessible and activated by their environment. This is a mechanism of action reminiscent of enzyme-suicide inhibition. These characteristics may be a useful paradigm for development of new selective NR antagonists.

RESULTS

Reaction of the TRβ LBD with DHPPA

To understand the mechanism of reaction between DHPPA and TRβ, we carried out several studies to determine the reactivity of individual LBD-exposed cysteine residues and the degree to which unbound HPPE is generated. If HPPE is generated locally and reacts with an immediately adjacent sulfhydryl then DHPPA activity should be resistant to exogenous thiols in the buffer, and the majority of the conjugated HPPE should be directed to the TRβ. Indeed, when coactivator-binding experiments were carried out in the presence of increasing amounts of β-mercaptoethanol (BME, 10 nM to 10 mM), no "external product" resulting from the conjugation of HPPE with BME was detected by mass spectrometry (See Supplementary Materials). Additionally, the DHPPA inhibitor remained fully active with no shifts in potency or efficacy until the concentration of BME exceeded 10 mM (a roughly 20,000-fold excess relative to protein). These findings suggest that the HPPE is generated within the binding site and remains bound to that site until it reacts with one of the local cysteines.

We also assessed the sensitivity of TRβ to non-specific alkylators that attack surface-exposed sulfhydryls to determine whether a particularly reactive cysteine residue was present or if the protein was particularly sensitive to electrophiles. To assess these issues, we conducted coactivator-binding experiments in the presence of increasing concentrations (10 nM to 10 mM) of the sulfhydryl-reactive reagents iodoacetamide and N-ethylmaleimide.

Neither of these reagents had strong influence on the behaviour of TRβ. In fact, no difference in coactivator binding was detected for either reagent until its concentration exceeded 100 μM (iodoacetamide) and 1 mM (N-ethylmaleimide), which relative to the amounts of protein present were about 1000-fold and 10,000-fold excess, respectively. The potency of iodoacetamide was also approximately 100-fold lower than that of DHPPA or HPPE, and the potency of N-ethylmaleimide was 1000-fold lower. These findings imply that some characteristic of HPPE provides a specific alkylation event that blocks function.

In addition to these experiments, we re-examined previously published high resolution TR crystal structures resulting from crystals that had been soaked with or grown in the presence of such vast excesses of non-specific alkylators (PDB IDs 2H6WX, 2H77A, 2H79A and others). Surface exposed cysteine residues in these structures were found to have reacted with buffer components and there was an even distribution of alkylation events among exposed cysteines of Cys294, Cys298, Cys388, Cys434 and their TRα equivalents. Together, these findings imply that the inactivation of TRβ by DHPPA is the result of a specific, targeted alkylation event that results from interaction of the particular electrophile with the protein surface, probably through positioning of the electrophilic pharmacophore element and not due to a particularly reactive cysteine residue.

Structure of the TRβ LBD-Ketone Complex

To understand how DHPPA inhibits coactivator binding to TRβ, we set out to image the compound at the TR surface. Attempts to co-crystallize TRβ LBD in complex with the TH Triac (3,3',5-triiodothyroacetic acid) and DHPPA were not successful. We therefore first obtained crystals of a TRβ mutant (TRβ D355R) in complex with Triac and then soaked crystals for varying times with DHPPA solutions, as described in the Methods. This TRβ mutant formed stable dimers in solution but otherwise displayed normal transcriptional activity [(31) and in preparation] and was chosen here because it forms long-lived crystals that are relatively stable (data not shown).

Long-term treatment of preformed TRβ D355R:Triac crystals with DHPPA solution resulted in significant dimensional changes in the lattice. Crystals failed to diffract beyond 10 Å when soaked for 2 hours. Crystals that were soaked with DHPPA for as long as 1 hour diffracted to 2.3 Å, thereby permitting structural analysis and assignment of the compound to the TR surface. The secondary and tertiary structures of the TRβ D355R mutant were identical to those of wild-type TRs. Two molecules of TRβ D355R formed a dimer (monomer A and B) with a root mean square between monomers of 0.47 Å; Triac was buried inside the ligand-binding pocket. Given extensive similarities between this and previously elucidated TR structures (32-34), the details of TRβ LBD organization will not be further described.

We detected a single compound at the TR AF-2 surface. Consistent with our predicted mechanism, this was HPPE, the product of DHPPA β-elimination, and not the parental DHPPA compound that was utilized in the soaks (Fig. 1). HPPE has three pharmacophore components: a hydrophobic alkyl chain, a hydrophobic benzyl ring and a hydrophilic unsaturated ketone substituent that comprises the reactive site. All of these features were clearly visible. No evidence indicated the presence of the amine group that is characteristic of DHPPA. We were not able to detect DHPPA or HPPE binding to any other region of the TR LBD surface. Our analysis of the relative electron densities of the compound and receptor suggested that there was 1:1 stoichiometry.

As observed in the crystal structure, HPPE was unreacted with TR but positioned close to several cysteine residues (Fig. 2). As described above, TRβ AF-2 is a small concave surface that contains the following six hydrophobic residues that are essential for coactivator recruitment: V284, K288, I302, K306, L454, and E457. The HPPE alkyl chains bind to a hydrophobic patch formed by L454 and V284; the aromatic ring binds to the concave AF-2 surface, making contacts with L454, V284, and I302. The ketone carbonyl oxygen engages in a water-mediated

electrostatic interaction with the K306 amino group, though the distance between these residues (5.7 Å) and that from E457 (about 5.5 Å) eliminates the possibility of a true hydrogen bond forming. Overall, these interactions guide the reactive hydrophilic portion of the HPPE molecule close to four cysteine residues. The unsaturated enone part of the molecule lies about 6.5 Å from Cys309, which is located in the base of the AF-2 cleft. The side chain of Cys308 is buried within the core of the domain with side chain atoms and main chain atoms forming a separation wall between it and the enone. The reactive group of HPPE also lies within 10 Å of Cys298 and Cys294, which are represented on the upper right and right corners of the AF-2 site.

Together, our results suggest that HPPE is liberated from DHPPA in the TRβ crystal and stably binds within the AF-2 cleft. Previous chemical analyses showed that HPPE binds irreversibly to the TRβ LBD with strong time dependency(21). The fact that our crystal contains an unreacted HPPE molecule suggests that the structure corresponds to an intermediate stage of this two-step reaction.

Identification of Covalent Attachment Sites of HPPE on TRβ LBD

To understand how HPPE inhibits TR AF-2 activity, we set out to identify the most likely target(s) of HPPE modification using mass spectrometry of treated protein. Trypsin-digested control and HPPE-treated protein samples were used to define the precise site(s) on TR that was modified by treatment with HPPE. We analyzed the resulting peptides by nanoscale liquid chromatography coupled online to a tandem mass spectrometer. Fragmentation spectra were acquired automatically and interpreted manually and via the use of the MASCOT protein database searching program (Matrix Science, Boston, MA). Alkylation by HPPE was observed in a peptide spanning residues 289 to 306 (KLPMFCELPCEDQIILLK) (Fig. 3). Fragmentation spectra were obtained for both the $[M+2H]^{2+}$ and $[M+3H]^{3+}$ precursor ion forms, and in both cases, Cys298 was conclusively shown to be the site of modification. Comparison of the integrated ion intensities from the normal and modified forms of this peptide suggested stoichiometric modification at this site; however, possible differences in the relative ability of the two species to ionize precluded a quantitative appraisal of the extent of modification

Despite observing peaks corresponding to fragment peptides spanning most of the HPPE-binding site, we did not observe peptides that included Cys308 and/or Cys309 in either the control or experimental samples. Thus, although Cys298 is readily modified by HPPE, we cannot rule out some degree of reaction with Cys309 or its neighbor. Nevertheless, mass spectrometry did confirm that Cys294 was unreacted.

Two other sites were modified at very low stoichiometry (< 0.1), Lys211 and Cys388. Lys211 is a highly accessible residue located at the beginning of the N-terminal fragment of the LBD TRβ structure, before helix 1. It is fully solvent accessible, and it is not located in any secondary structure element. Cys388 is also surface exposed and located at the C terminus of helix 9, on the opposite side of the receptor from AF-2. Together, our results suggest that Cys298, which is adjacent to the AF-2 surface, is the major target for HPPE modification.

Mutation of Cys 298 Creates a TR that Binds Coactivators but is Resistant to DHPPA

To assess the role of Cys298 in DHPPA inhibition of TR activity, we determined the effect of mutation of Cys298 on cofactor binding and DHPPA reactivity. Significant amounts of T_3-liganded wild-type TRβ were retained on an affinity column in which the NR-interaction domain of the coactivator SRC2 was attached to the solid support (Fig. 4). TRβ alone (i.e., uncoupled from its ligand) did not bind to the column (data not shown). Incubation with increasing amounts of DHPPA or HPPE inhibited TRβ binding to its coactivator SRC2 in a dose-dependent manner, whereas an unreactive control compound 1-(4-hexylphenyl)propan-1-one (HPPA) did not. In parallel, a TRβ mutant in which serine was substituted for Cys298 (C298S) bound strongly to the column, confirming that this residue is not needed for TRβ to bind the coactivator and is insensitive to

DHPPA and HPPE action. Thus, Cys298 is not required for cofactor binding but is necessary for DHPPA activity.

To explore the roles of the cysteine residues located near the AF-2 pocket in DHPPA action, we examined the effects of mutations that targeted key residues surrounding the AF-2 surface but permitted some cofactor binding. Cys298 mutations C298S and C298R suppressed the ability of DHPPA to inhibit cofactor binding, whereas a mutation at Cys294 (C294K) did not (Fig. 5, upper panel). A mutation of Cys309 (C309A) that permitted coactivator binding also failed to reverse the ability of DHPPA to inhibit SRC2 binding (Fig. 5, lower panel).

Both the elimination of DHPPA to form HPPE and the reaction of DHPPA with nucleophilic groups at the TR surface should be affected by mutations that alter the electrostatic environment at the reaction site. Not surprisingly, mutations in charged residues that surround the AF-2 cleft modestly reduced the efficacy of DHPPA. Removal of the positive charge at lysine residue 306 reduced the efficacy of DHPPA (Fig. 5, lower panel), even though we did not detect modification of this residues in mass spectroscopic analysis. In contrast, removal of the charge at glutamate residue 457 or lysine 288 on H12 had no effect (Fig. 5, lower panel).

DHPPA inhibits TRβ Binding to the NR Corepressor

Coactivators and corepressors bind to an overlapping TR surface that comprises most of the H3-H5 region of the AF-2 surface (15, 24) but differ in their requirements for H12. DHPPA and HPPE inhibited TRβ coactivator binding via a mechanism that involves attachment to AF-2 and modification of Cys298; thus, we examined the effects of DHPPA on corepressor binding.

Results from our pull-down assays suggested that DHPPA inhibits NR corepressor (N-CoR) binding via a mechanism that is similar to its effects on coactivator binding. DHPPA inhibited interactions between wild-type TRβ alone (i.e., uncoupled from its ligand) and N-CoR. The C298R mutation did not inhibit corepressor binding but rendered the receptor insensitive to DHPPA, whereas the C309A mutation had no obvious effect on DHPPA action (Fig. 6). In addition, a mutation at residue 451 (451X) that truncated H12 and permitted strong corepressor binding by exposing the complete N-CoR–binding surface (24) did not affect the sensitivity of TRβ to DHPPA (Fig. 6). Thus, DHPPA inhibits TRβ interactions with corepressors via a mechanism that requires Cys298 but is independent of H12.

DISCUSSION

In this paper, we report the X-ray structure of TRβ in complex with our prototype SID, DHPPA, at 2.3-Å resolution. In addition, results of our mass spectroscopic and mutational analyses reveal that the primary target of DHPPA is a specific cysteine residue (Cys298). These combined structural and functional data also indicate that DHPPA is a prodrug that produces the active compound HPPE by β-elimination, and HPPE specifically targets cysteines in the binding interface. The resulting covalent complex is then unable to recruit coregulators.

Our X-ray structure of TRβ in complex with HPPE confirms that our lead compound interacts specifically with AF-2. We observed a single HPPE molecule that binds to the TRβ AF-2 surface with 1:1 stoichiometry, and there is no evidence that the compound binds elsewhere. The structure also confirms our prediction that DHPPA liberates a reactive intermediate (HPPE) that is in contact with the TRβ surface. Although we incubated TRβ-Triac crystals with the parental β-amino-ketone DHPPA, the α,β-unsaturated ketone HPPE bound to the TRβ AF-2 pocket. Nevertheless, we did not detect electron density that would be consistent with a covalent bond forming between the unsaturated part of HPPE and nearby cysteine residues. Finally, biochemical experiments indicated that little, if any, HPPE escapes into solution. Thus, our structure probably represents a reaction intermediate in which the active form of the compound interacts with TRβ but has not yet completed reaction with the receptor surface.

Functional analysis indicates that the

major target for HPPE modification is Cys298, which lies close to the AF-2 cleft. Mass spectroscopic analysis reveals that this residue is modified by HPPE at stoichiometric levels in solution. Moreover, Cys298 mutations uniquely render TRβ insensitive to DHPPA and HPPE action, as revealed by inhibition of TRβ interactions with SRC2 and NCoR in pull-down assays. Although we mostly detect modification at Cys298, HPPE is not completely specific; there are low levels of modification at Lys211 and Cys388. In addition, we were not able to detect tryptic peptides that overlap Cys309 by mass spectroscopic analysis, so we are not yet able to rule out the possibility that HPPE reacts with this residue at low levels. Nevertheless, Cys309 mutations do not affect DHPPA and HPPE action, suggesting that this residue is not an important target for these SIDs. Supporting a specific molecular mode of action, none of these residues is highly reactive with non-specific electrophiles.

Together, our findings suggest a likely mechanism for DHPPA action. We postulate that the time dependency of the reaction and the loss of diffraction in the crystal are indicative of a two-step binding mode. The first step is reversible binding of HPPE in the AF-2 pocket, with orientation of the unsaturated part of the ketone toward the nearby nucleophilic side chain of Cys298. After effective positioning, the second step, a slow interconversion of this complex to the covalent adduct, alters the structure sufficiently to prevent formation of diffracting crystals. Because Cys298 is dispensable for coactivator binding to TRβ *per se* but is absolutely required for HPPE action, the formation of the Cys298/HPPE adduct most likely interferes in a steric manner with coactivator binding to the AF-2 cleft. Prolonged soaking destroys the crystals; therefore, we believe that other residues, probably those identified by mass spectrometry, are sufficiently reactive to be alkylated and damage lattice associations.

Some aspects of the reaction mechanism remain unclear. First, we do not know whether the conversion of DHPPA to HPPE occurs in solution with subsequent binding to TRβ AF-2, or whether it takes place at the AF-2 surface. Mannich base elimination occurs slowly in solution and rapidly at protein surfaces; thus, we favour the latter possibility. This is bolstered by the fact that we do not detect the expected "external" products of reaction between buffer components and HPPE. When bound in the mode shown in our structure, the ketone carbonyl oxygen is 5.5 Å from Glu457, and the ketone α-carbon is 5.7 Å from Lys306. This structure raises the possibility that these charged residues facilitate the β-elimination reaction. If so, then the nature of the TRβ active site may play an important role in reactivity of the compound. Second, it is not obvious why Cys298 is the preferred target for modification. There are four possible target cysteine residues near AF-2. Our structure reveals that the reactive group of HPPE is not positioned appropriately to modify Cys294 and that Cys308 is buried in the core of the receptor. Furthermore, Cys309 lies at the base of AF-2 close to HPPE's unsaturated ketone group. It is not clear why this residue is not important for HPPE action. Perhaps dynamic structural alterations that affect the organization of the AF-2 cleft and are apparent in comparisons of TRα and TRβ structures (21) render the Cys309 side chain inaccessible for HPPE modification in solution.

We expect that our results will facilitate the development of improved second-generation SIDs for TRs. Although DHPPA and HPPE are relatively specific inhibitors of TRβ, they are not potent enough to be useful TR antagonists in the therapeutic setting. Our structural and functional analyses reveal important features of the TR surface that are needed for HPPE binding and action. The TRβ AF-2 pocket contains a narrow hydrophobic passageway that leads to a defined subpocket featuring Cys309 at its bottom, charge beacons provided by Glu457 and Lys306 at its rim, and a flatter subsite surrounded by Cys298 and Lys288. HPPE exploits these topologic features to bind TRβ. The compound is captured by the concerted binding of the alkyl chain into the hydrophobic passageway and the aromatic enone moiety into the deep concave hole; the compound targets Cys298, which flanks the flatter hydrophobic subsite. Furthermore, mutational analysis reveals an important but undefined role for Lys306 in DHPPA action; these include possibly orienting the molecule in

the appropriate manner for cysteine modification or facilitating elimination of the parental compound, DHPPA. Furthermore, our analysis also suggests ways to improve HPPE binding. Interactions with the flatter AF-2 subsite that is surrounded by Cys298 and Lys288 appear to be suboptimal, and the compound does not bind at all to a large part of the coactivator-binding surface bridged by Glu285. In addition, the fact that DHPPA inhibits TRβ/N-CoR interactions in a manner that is independent of H12 implies that this helix must be dispensable for DHPPA and HPPE action. Thus, chemical modifications that preserve hydrophobic and polar interactions revealed in our structure while simultaneously enhancing suboptimal interactions of HPPE with unoccupied regions of the AF-2 surface and H12 should increase DHPPA's affinity for TRβ and improve its specificity.

Because it was possible to identify at least one SID that binds specifically to the TRβ AF-2 surface, we expect that we will identify similar inhibitors that bind to the AF-2 of other NRs or perhaps to alternate hydrophobic interaction surfaces such as dimer sites. Given the likely complexity and dynamic nature of such protein-interaction surfaces, we do not think that it will be easy to identify these compounds with standard computer-based molecular modelling approaches. Instead, we suggest that high-throughput screening approaches will identify useful leads and that a combination of X-ray structural analysis and further chemical modification will yield SIDs with high specificity for NRs. Given the mechanism of action of HPPE outlined here, we suggest that NRs with adventitiously placed cysteine residues in close proximity to protein-interaction surfaces would be useful targets.

In summary, few molecules are known to interrupt protein-protein interactions, and of those, the structures of only a few have been characterized. This study presents the first crystal structure of a small molecule that binds to an NR AF-2 pocket, inhibits transcription through its interactions at the AF-2 pocket, and provides important guidelines for future development of improved versions of such compounds. Molecules such as DHPPA and HPPE are the first members of a new class of NR antagonists that are active in the presence of hormone and will provide new options for manipulating the actions of these receptors.

MATERIALS AND METHODS

Protein Expression and Purification

The hTRβ (D355R) LBD (His_6 E209-D461) cDNA sequences were cloned into the BamHI and HindIII restriction sites downstream of the hexahistidine tag of the expression vector pETDuet-1 (Novagen, Madison, WI). The replacement of Asp355 for arginine in the hTRβ LBD construct was performed with the QuickChange XL Site-Directed Mutagenesis Kit (Stratagene, La Jolla, CA). The sequence was verified by DNA sequencing (Elim Biopharmaceuticals, Inc., Hayward, CA).

The hTRβ (D355R) LBD was expressed in BL21(DE3) cells added at OD_{600} = 0.6). When the OD_{600} reached four, cells were harvested, resuspended in 20 ml buffer per 1 L culture medium (20 mM Tris, 300 mM NaCl, 0.025% Tween-20, 0.10mM PMSF, 10 mg of lysozyme, pH 7.5) incubated for 30 min on ice, and then sonicated three times for 3 min on ice. The lysed cells were centrifuged at 100,000 x *g* for 1 h, and the supernatant was loaded onto Talon resin (20 mL; Clontech, Mountain View, CA). Protein was eluted with 500 mM imidazole (3 × 5 mL) plus ligand [3,3',5-triiodo-L-thyronine (Sigma, St. Louis, MO)]. Protein purity (>90%) was assessed by SDS-PAGE and high-performance size-exclusion chromatography (HPSEC), and protein concentration measured by the Bradford protein assay. The protein was dialyzed overnight against assay buffer (3 × 4 L, 50 mM sodium phosphate, 150 mM NaCl, pH 7.2, 1 mM DTT, 1 mM EDTA, 0.01% Nonidet P-40, and 10% glycerol).

Crystallization, Structure Determination, and Refinement

A pre-grown TRβ LBD crystal was soaked with 3 μL of a 10mM DHPPA compound solution in DMSO for 1 h. The crystal was obtained by vapor-diffusion methods (hanging-drop technique) in 25% ethylene

glycol. The protein solution (1 μL) was mixed with 1 μL of the reservoir solution and concentrated against 300 μL of the reservoir. The crystal was flash-cooled using liquid nitrogen and measured using the synchrotron radiation at the 8.3.1 beam line at the Advanced Light Source (University of California, Berkeley), where a complete dataset was collected at 2.3-Å resolution.

The crystal belongs to space group $P2_1$ and contains two molecules per asymmetric unit. The diffraction data were integrated and scaled using the computer program ELVES (UC Berkley) (35). Molecular-replacement solution for the TRβ LBD structure was obtained using rotation and translation functions from Crystallography & NMR Systems (36). The first electron maps calculated after the rigid body refinement that followed the molecular replacement displayed clear electron density for the compound and less-defined density indicating flexibility for its alkyl chain. During the improvement of the protein model, the Fourier maps revealed perfectly traceable electron density for the entire compound. A composite-omit map that did not include the compound was calculated during refinement for overcoming phase bias. This map was calculated by omitting 5% of the total model, thereby allowing a better tracing of the main alkyl-chain in the compound. Model building was done using QUANTA software (Accelrys Software, San Diego, CA), which was monitored using the R-free factor.

Calculation of the electron density maps and crystallographic refinement was performed with CNS software (Crystallography & NMR Systems, Cary, NC) using the target parameters of Engh and Huber (37). Several cycles of model building, conjugate gradient minimization, and simulated annealing using CNS resulted in structures with good stereochemistry. A Ramachandran plot showed that most of the residues fall into the most favored or allowed regions. The statistics for data collection and refinement are presented in Table 1. The structure has been deposited with the Protein Data Bank (PDB) and assigned the following ID number: PDB ID 2F9E, RCSB ID RCSB035615.

Pre-grown TRβ crystals soaked with the same 10 mM HPPE compound solution in DMSO for longer than 1h failed to diffract beyond 10-Å resolution at Advanced Light Source.

Tandem Mass Spectrometric Analysis:

TRβ sample in buffer (3 × 4 L, 50 mM sodium phosphate, 150 mM NaCl, pH 7.2, 1 mM DTT, 1 mM EDTA, 0.01% Nonidet P-40, and 10% glycerol) was denatured by addition of 8 M urea, diluted to 1 M urea, and then digested overnight by addition of trypsin at 1:50 ratio by mass. The resulting peptides were subjected to nanoscale LC/MS/MS analysis using a QTrap mass spectrometer (Applied Biosystems/Sciex, Foster City, CA) coupled to an LC Packings UltiMate™ on-line reverse-phase chromatography system (Dionex, Sunnyvale, CA). Peptides were eluted over the course of 2 h by using a gradient of 5% to 30% acetonitrile at a flow rate of 150 nL/min. Peptide-fragmentation spectra were automatically acquired using the "Enhanced Product Ion" scan modality. The resulting data were analysed using MASCOT software (Matrix Science). The software was asked to consider possible HPPE-mediated alkylation of cysteine and lysine residues.

Pull-down Assays

TRβ labeled with ^{35}[S] methionine was produced *in vitro* using the TNT-Coupled Reticulocyte Lysate System (Promega, Madison, WI). The GST fusions were expressed in *E. coli* BL21 purified, and anchored to a solid support (agarose-glutathione beads) according to the manufacturer's instructions. For binding assays, bead suspensions containing 10 μg GST fusion protein were incubated with 3 μL ^{35}[S]-labeled wild-type or mutant TRβ in 150 μL IPAB-80 buffer containing 2 μg/mL BSA, 10^{-6} M T_3, and various concentrations of DHPPA, HPPE, or controls. After incubation for 2 h at 4 °C, beads were washed (three times) with 1 mL IPAB-80 buffer and heated to 100 °C for 3 min. Bound proteins were

separated by SDS-PAGE (10% polyacrylamide) and visualized by autoradiography and quantified on a Kodak M1 apparatus with Molecular Imaging software.

Acknowledgements

We thank Elena Sablin for useful discussions. James Holton and George Meigs for assistance with crystallization data collection and processing at the Advanced Light Source 8.3.1 beamline (UC Berkeley), and A J McArthur in Scientific Editing at SJCRH for comments on the manuscript. .

Note: The compounds DHPPA and HPPE were named generically L1 and L3, respectively (21). Their official names are SJ-000000001 and SJ-000000002, respectively. The compound HPPA is officially named SJ-000000055.

ABBREVIATIONS

AF, activation function
AR, androgen receptor
CNS, Crystallography & NMR Systems
DHPPA, 3-(dibutylamino)-1-(4-hexylphenyl)propan-1-one
DMSO, dimethylsulfoxide
DTT, dithiothreitol
ER, estrogen receptor
GST, glutathione S-transferase
HNF-4α, hepatocyte nuclear factor 4α
HPPA, 1-(4-hexylphenyl)propan-1-one
HPPE, 1-(4-hexylphenyl)prop-2-en-1-one
HPSEC, high-performance size-exclusion chromatography
IC_{50}, inhibitory concentration
LBD, ligand-binding domain
LC-MS/MS, liquid chromatography, mass spectrometry
LXXLL, leucine-x-x-leucine-leucine
NaCl, sodium chloride
N-CoR, nuclear receptor corepressor
NR, nuclear hormone receptor
Nurr1, orphan nuclear receptor 1
PDB, Protein Data Bank
PMSF, phenylmethylsulphonylfluoride
SID, surface interacting drugs
SRC2, steroid receptor coactivator 2
TH, thyroid hormone
TR, thyroid receptor
Triac, 3,3',5-triiodothyroacetic acid

REFERENCES

1. Mangelsdorf DJ, Thummel, C., Beato, M., Herrlich, P., Schutz, G., Umesono, K., Blumberg, B., Kastner, P., Mark, M., Chambon, P., Evans, R.M. 1995 The Nuclear Receptor Superfamily: the Second Decade. Cell 83:835-839
2. Evans R 2005 The nuclear receptor superfamily: a rosetta stone for physiology. Mol Endocrinol 19:1429-1438
3. Schiff R, Massarweh, S., Shou, J., and Osborne K.C. 2003 Breast Cancer Endocrine Resistance.How Growth Factor Signaling and Estrogen Receptor Coregulators Modulate Response. Clinical Cancer Research 9
4. Klotz L, Schellhammer, P. 2005 Combined androgen blockade: the case for bicalutamide. Clin Prostate Cancer 3:215-219
5. Schellhammer P 1999 An update on bicalutamide in the treatment of prostate cancer. Expert Opin Investig Drugs 8:849-860
6. Milliez P, Deangelis, N., Rucker-Martin, C., Leenhardt, A., Vicaut, E., Robidel, E., Beaufils, P., Delcayre, C., Hatem, S.N. 2005 Spironolactone reduces fibrosis of dilated atria during heart failure in rats with myocardial infarction. Eur Heart J 26:2193-2199
7. Gemzell-Danielsson K, Marions, L. 2004 Mechanisms of action of mifepristone and levonorgestrel when used for emergency contraception. Hum Reprod Update 10:341-348
8. Webb P NN, Chiellini G, Yoshihara HA, Cunha Lima ST, Apriletti JW, Ribeiro RC, Marimuthu A, West BL, Goede P, Mellstrom K, Nilsson S, Kushner PJ, Fletterick RJ, Scanlan TS, Baxter JD. 2002 Design of thyroid hormone receptor antagonists from first principles. J Steroid Biochem Mol Biol 83:59-73
9. Nguyen NH, Apriletti, J.W., Cunha-Lima, S.T., Webb, P., Baxter, J.D., Scanlan, T.S. 2002 Rational design and synthesis of a novel thyroid hormone antagonist that blocks coactivator recruitment. J Med Chem 45:3310-3320
10. Jenster G, van der Korput JA, Trapman J, Brinkmann AO 1992 Functional domains of the human androgen receptor. J Steroid Biochem Mol Biol 41:671-675
11. Warnmark A, Gustafsson JA, Wright AP 2000 Architectural principles for the structure and function of the glucocorticoid receptor tau 1 core activation domain. J Biol Chem 275:15014-15018
12. Demarest SJ, Martinez-Yamout, M,, Chung, J., Chen, H., Xu, W., Dyson, H.J., Evans, R.M., Wright, P.E. 2002 Mutual synergistic folding in recruitment of CBP/p300 by p160 nuclear receptor coactivators. Nature 415:549-553.
13. Warnmark A, Treuter E, Wright AP, Gustafsson JA 2003 Activation functions 1 and 2 of nuclear receptors: molecular strategies for transcriptional activation. Mol Endocrinol 17:1901-1909
14. Baxter JD, Goede, P., Apriletti, J.W., West, B.L., Feng, W., Mellstrom, K., Fletterick, R.J., Wagner, R.L., Kushner, P.J., Ribeiro, R.C., Webb, P., Scanlan, T.S., Nilsson, S. 2002 Structure-based design and synthesis of a thyroid hormone receptor (TR) antagonist. Endocrinology 143:271-286
15. Darimont BD, Wagner, R. L., Apriletti, J. W., Stallcup, M. R., Kushner, P. J., Baxter, J. D., Fletterick, R. J., Yamamoto, K. R. 1998 Structure and specificity of nuclear receptor-coactivator interactions. Genes Dev 12:3343-3356
16. Darimont BD, Wagner RL, Apriletti JW, Stallcup MR, Kushner PJ, Baxter JD, Fletterick RJ, Yamamoto KR 1998 Structure and specificity of nuclear receptor-coactivator interactions. Genes Dev 12:3343-3356

17. Zhou Y, Eppenberger-Castori, S., Eppenberger, U., Benz, C.C. 2005 The NFkappaB pathway and endocrine-resistant breast cancer. Endocr Relat Cancer 12:S37-46
18. Damber JE 2005 Endocrine therapy for prostate cancer. Acta Oncol 44:605-609
19. Wang Z, Benoit, G., Liu, J., Prasad, S., Aarnisalo, P., Liu, X., Xu, H., Walker, N.P., Perlmann, T. 2003 Structure and function of Nurr1 identifies a class of ligand-independent nuclear receptors. Nature 423:555-560
20. Estebanez-Perpina E, Moore, J.M., Mar, E., Delgado-Rodrigues, E., Nguyen, P., Baxter, J.D., Buehrer, B.M., Webb, P., Fletterick, R.J., Guy, R.K. 2005 The molecular mechanisms of coactivator utilization in ligand-dependent transactivation by the androgen receptor. J Biol Chem 280:8060-8068
21. Arnold LA, Estebanez-Perpina, E., Togashi, M., Jouravel, N., Shelat, A., McReynolds, A.C., Mar, E., Nguyen, P., Baxter, J.D., Fletterick, R.J., Webb, P., Guy, R.K. 2005 Discovery of small molecule inhibitors of the interaction of thyroid hormone receptor with transcriptional coregulators. J Biol Chem
22. Arnold LA, Estebanez-Perpina, E., Togashi, M., Shelat, A., Ocasio, C.A., McReynolds, A.C., Nguyen, P., Baxter, J.D., Fletterick, R.J., Webb, P., Guy, R.K. 2006 A high-throughput screening method to identify small molecule inhibitors of thyroid hormone receptor coactivator binding. Sci STKE 341:13
23. Hur E, Pfaff SJ, Sturgis PE, Hanne G, Buehrer BM, Fletterick RJ 2004 Recognition and Accommodation at the Androgen Receptor Coactivator Binding Interface. PLoS 2:363
24. Feng W, Ribeiro RC, Wagner RL, Nguyen H, Apriletti JW, Fletterick RJ, Baxter JD, Kushner PJ, West BL 1998 Hormone-dependent coactivator binding to a hydrophobic cleft on nuclear receptors. Science 280:1747-1749
25. Collingwood TN, Wagner R, Matthews CH, Clifton-Bligh RJ, Gurnell M, Rajanayagam O, Agostini M, Fletterick RJ, Beck-Peccoz P, Reinhardt W, Binder G, Ranke MB, Hermus A, Hesch RD, Lazarus J, Newrick P, Parfitt V, Raggatt P, de Zegher F, Chatterjee VK 1998 A role for helix 3 of the TRbeta ligand-binding domain in coactivator recruitment identified by characterization of a third cluster of mutations in resistance to thyroid hormone. Embo J 17:4760-4770
26. Becerril J, Hamilton AD 2007 Helix Mimetics as Inhibitors of the Interaction of the Estrogen Receptor with Coactivator Peptides. Angew Chem Int Ed Engl 46:4471-4473
27. Rodriguez AL, Tamrazi A, Collins ML, Katzenellenbogen JA 2004 Design, synthesis, and in vitro biological evaluation of small molecule inhibitors of estrogen receptor alpha coactivator binding. J Med Chem 47:600-611
28. Shao D, Berrodin TJ, Manas E, Hauze D, Powers R, Bapat A, Gonder D, Winneker RC, Frail DE 2004 Identification of novel estrogen receptor alpha antagonists. J Steroid Biochem Mol Biol 88:351-360
29. Wang Y, Chirgadze, N.Y., Briggs, S.L., Khan, S., Jensen, E.V,, Burris, T.P. 2006 A second binding site for hydroxytamoxifen within the coactivator-binding groove of estrogen receptor beta. Proc Natl Acad Sci U S A 103:9908-9911
30. Arend M, Westermann, B., Risch, N. 1998 Modern variants of the Mannich reaction. Angew Chem, Int Ed Engl 37:1045-1070
31. Togashi M, Nguyen, P., Fletterick, R., Baxter, J.D., Webb, P. 2005 Rearrangements in Thyroid Hormone Receptor Charge Clusters That Stabilize Bound 3,5',5-Triiodo-L-thyronine and Inhibit Homodimer Formation. J Biol Chem 280:25665-25673

32. Nascimento AS, Dias SM, Nunes FM, Aparicio R, Ambrosio AL, Bleicher L, Figueira AC, Santos MA, de Oliveira Neto M, Fischer H, Togashi M, Craievich AF, Garratt RC, Baxter JD, Webb P, Polikarpov I 2006 Structural rearrangements in the thyroid hormone receptor hinge domain and their putative role in the receptor function. Journal of molecular biology 360:586-598
33. Nunes FM, Aparicio R, Santos MA, Portugal RV, Dias SM, Neves FA, Simeoni LA, Baxter JD, Webb P, Polikarpov I 2004 Crystallization and preliminary X-ray diffraction studies of isoform alpha1 of the human thyroid hormone receptor ligand-binding domain. Acta Crystallogr D Biol Crystallogr 60:1867-1870
34. Wagner RL, Huber BR, Shiau AK, Kelly A, Cunha Lima ST, Scanlan TS, Apriletti JW, Baxter JD, West BL, Fletterick RJ 2001 Hormone selectivity in thyroid hormone receptors. Mol Endocrinol 15:398-410
35. Holton J, Alber, T. 2004 Automated protein crystal structure determination using ELVES. Proc Natl Acad Sci U S A 101:1537-1542
36. Brunger AT, Adams PD, Clore GM, DeLano WL, Gros P, Grosse-Kunstleve RW, Jiang JS, Kuszewski J, Nilges M, Pannu NS, Read RJ, Rice LM, Simonson T, Warren GL 1998 Crystallography & NMR system: A new software suite for macromolecular structure determination. Acta Crystallogr D Biol Crystallogr 54 (Pt 5):905-921
37. Engh RA, Huber, R. 1991 Accurate bond and angle parameters for X-ray protein structure refinement. Acta Crystallographica A47:392-400
38. DeLano WL 2002 The PyMOL Molecular Graphics System. In. San Carlos, CA, USA: DeLano Scientific

TABLE 1. Statistics for data collection and refinement of thyroid hormone receptor mutant TR-D355R crystals soaked with the unsaturated ketone HPPE

Measure	**Statistic**
No. of molecules per asymmetric unit	2
Space group	$P2_1$
Cell constants a/b/c	55.13 Å /92.87 Å /58.35 Å
β	109.65
Resolution	2.3 Å
No. of unique reflections	24,968
Completeness	
Overall	96.0%
Outermost shell	99.9%
R merge[a]	
No. of reflections used per refinement	24,966
Resolution range (Å)	500-2.29
R factor[b]	21.6%
R free[c]	25.6%
No. of water molecules	348
Matthews coefficient	2.34
Solvent content	47.59%
Ramachandran plot	
Most favored	92%
Allowed	7.5%

[a] R merge $= \sum hkl\ |<I>-I| / \sum_{hkl} |I|$

[b] R factor $= \sum_{hkl} ||Fo| - |Fc| / \sum_{hkl} |Fo|$

[c] R free set contained 5% of total data

FIGURE LEGENDS

FIGURE 1. Structures of inhibitors of the interaction of TRβ LBD and SRC2. A. The β-amino-ketone DHPPA [3-(dibutylamino)-1-(4-hexylphenyl)propan-1-one] was used in the soaking experiments.
B. The α,β-unsaturated ketone HPPE [1-(4-hexylphenyl)prop-en-1-one] was the compound seen in the structure.
C. The inactive compound HPPA [1-(4-hexylphenyl)propan-1-one] was used as the control.

FIGURE 2. Close-up of HPPE bound into the TRβ LBD AF-2 pocket.
A. Solid representation of TRβ LBD is depicted. The negatively charged residues are shown in red; the positively charged residues, in blue; the hydrophobic residues, in lilac; and the cysteine residues in yellow.
B. The TRβ AF-2 surface and the compound HPPE are shown as a grey stick model placed inside the AF-2 pocket. The distance between HPPE and K306 was 5.7 Å (white dotted line); that to E457, 5.7 Å (green dotted line); that to the unsaturated carbon and C309, 6.5 Å (black dotted line); and that to C298, 7.7 Å (yellow dotted line).
C. The TRβ AF-2 surface and the compound HPPE (shown as a grey stick model). A pale grey mesh is included to show the volume of the AF-2 pocket that the compound occupies. The figure was generated using PyMOL (38).

FIGURE 3. Mass spectrometric identification of HPPE modification of Cys298.
The fragmentation spectrum collected for a peptide spanning K289 to K306 and containing a covalent HPPE adduct at C298 is shown. The peptide ($[M+H]^+$: 2349.26) was observed as the triple-charged form ($[M+3H]^{3+}$: 784.3). The inset shows the peptide sequence and the observed y and b ion fragments. The modified cysteine is indicated in red.

FIGURE 4. Mutation at Cys298 abolishes the sensitivity of TRβ to DHPPA inhibition.
SDS-PAGE gel showing quantities of *in vitro*–translated T_3-liganded TRβ or the mutant TRβ C298S retained in pull-down assays using bacterially expressed GST-SRC2 (amino acids 563-1121) at 3 μg per assay. Binding is shown in assays performed with increasing concentrations (μM) of DHPPA, HPPE, or the control inactive compound HPPA.

FIGURE 5. Mutation at Cys298 but not at Cys309 uniquely abolishes DHPPA action.
Two SDS-PAGE gels showing quantities of *in vitro*–translated T_3-liganded wild-type (WT) TRβ or mutant TRs retained in pull-down assays using bacterially expressed GST-SRC2 (amino acids 563-1121) at 3 μg per assay in the presence of increasing concentrations (μM) of DHPPA

FIGURE 6. DHPPA inhibits corepressor N-CoR binding to TRβ.
SDS-PAGE gel showing quantities of *in vitro*–translated, unliganded wild-type (WT) TRβ or mutant TRs retained on GST–N-CoR (amino acids 1944-2453) in pull-down assays in the presence of increasing concentrations (μM) of DHPPA.

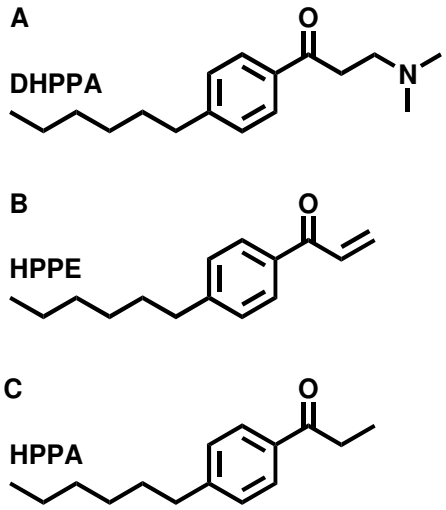
A
DHPPA
O
N
B
HPPE
O
C
HPPA
O

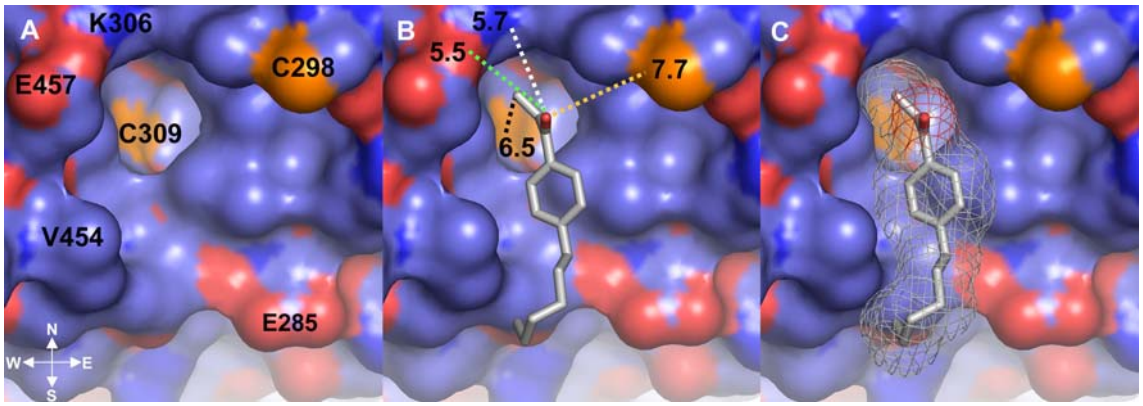
A
K306
E457
C298
C309
V454
E285
N
W
E
S
B
5.7
5.5
7.7
6.5
C

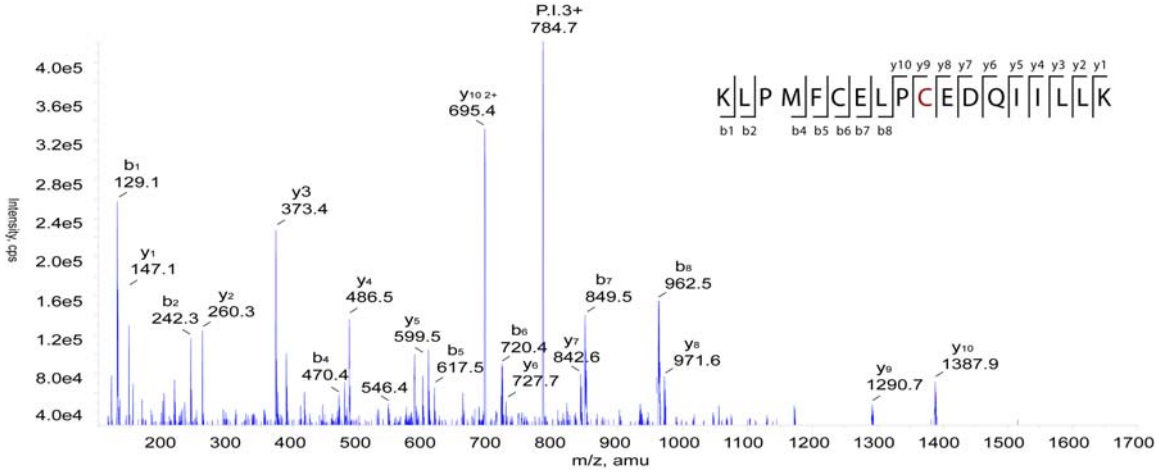
P.I.3+
784.7
y10 y9 y8 y7 y6 y5 y4 y3 y2 y1
K L P M F C E L P C E D Q I I L L K
b1 b2 b4 b5 b6 b7 b8
y10 2+
695.4
b1
129.1
y3
373.4
y1
147.1
b2
242.3
y2
260.3
y4
486.5
y5
599.5
b4
470.4
546.4
b5
617.5
b6
720.4
y6
727.7
y7
842.6
b7
849.5
b8
962.5
y8
971.6
y9
1290.7
y10
1387.9
Intensity, cps
4.0e5
3.6e5
3.2e5
2.8e5
2.4e5
2.0e5
1.6e5
1.2e5
8.0e4
4.0e4
200
300
400
500
600
700
800
900
1000
1100
1200
1300
1400
1500
1600
1700
m/z, amu

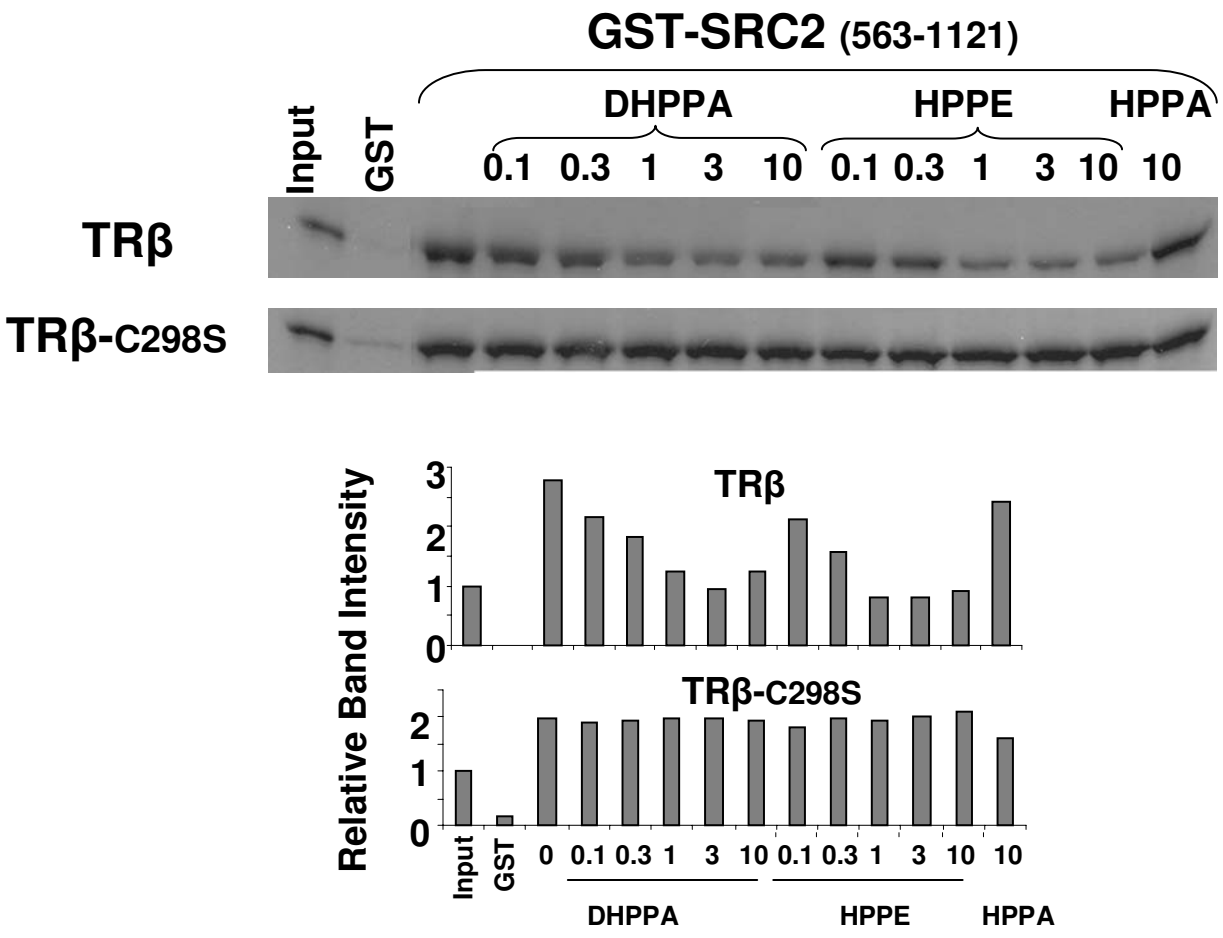
GST-SRC2 (563-1121)
Input
GST
DHPPA
HPPE
HPPA
0.1 0.3 1 3 10 0.1 0.3 1 3 10 10
TRβ
TRβ-C298S
Relative Band Intensity
TRβ
TRβ-C298S
0 0.1 0.3 1 3 10 0.1 0.3 1 3 10 10
DHPPA
HPPE
HPPA

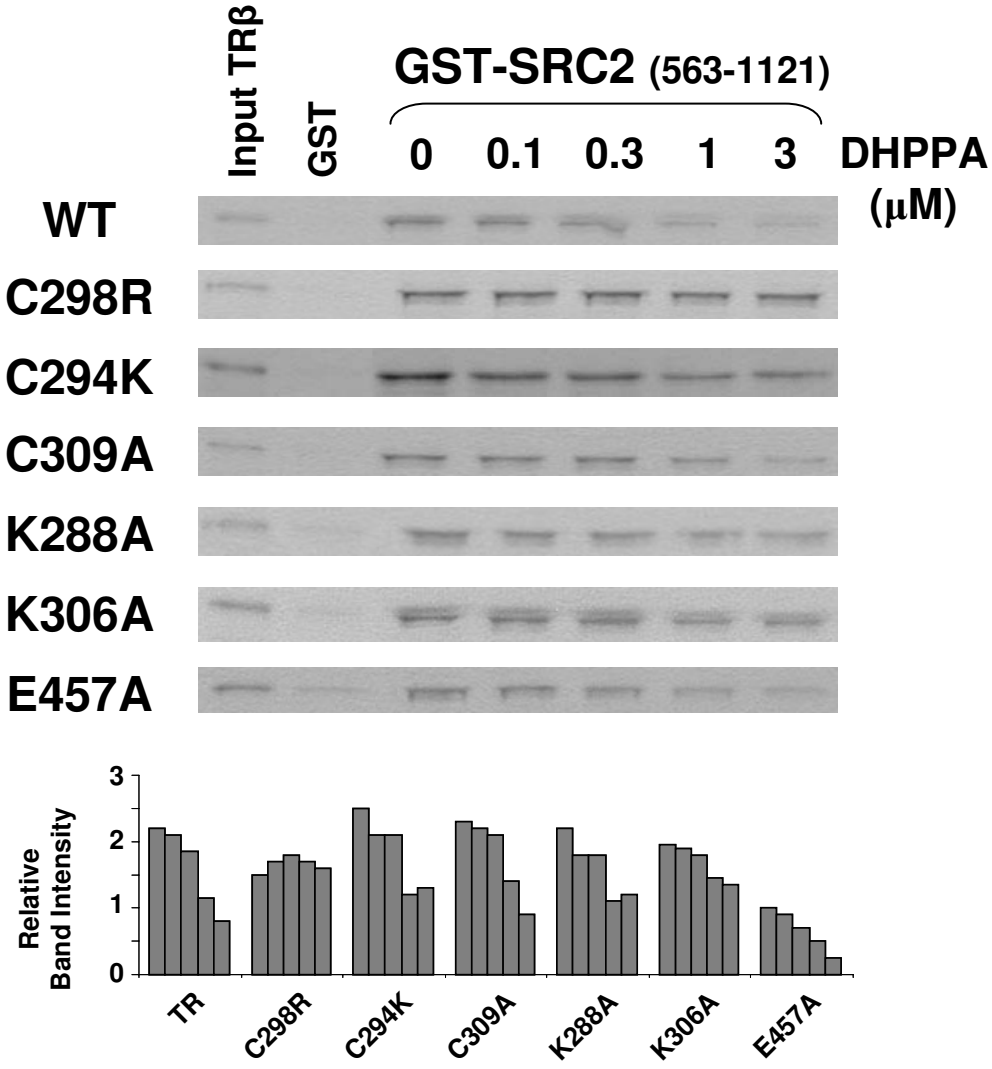
Input TRβ
GST
GST-SRC2 (563-1121)
0
0.1
0.3
1
3
DHPPA (μM)
WT
C298R
C294K
C309A
K288A
K306A
E457A
Relative Band Intensity
3
2
1
0
TR
C298R
C294K
C309A
K288A
K306A
E457A

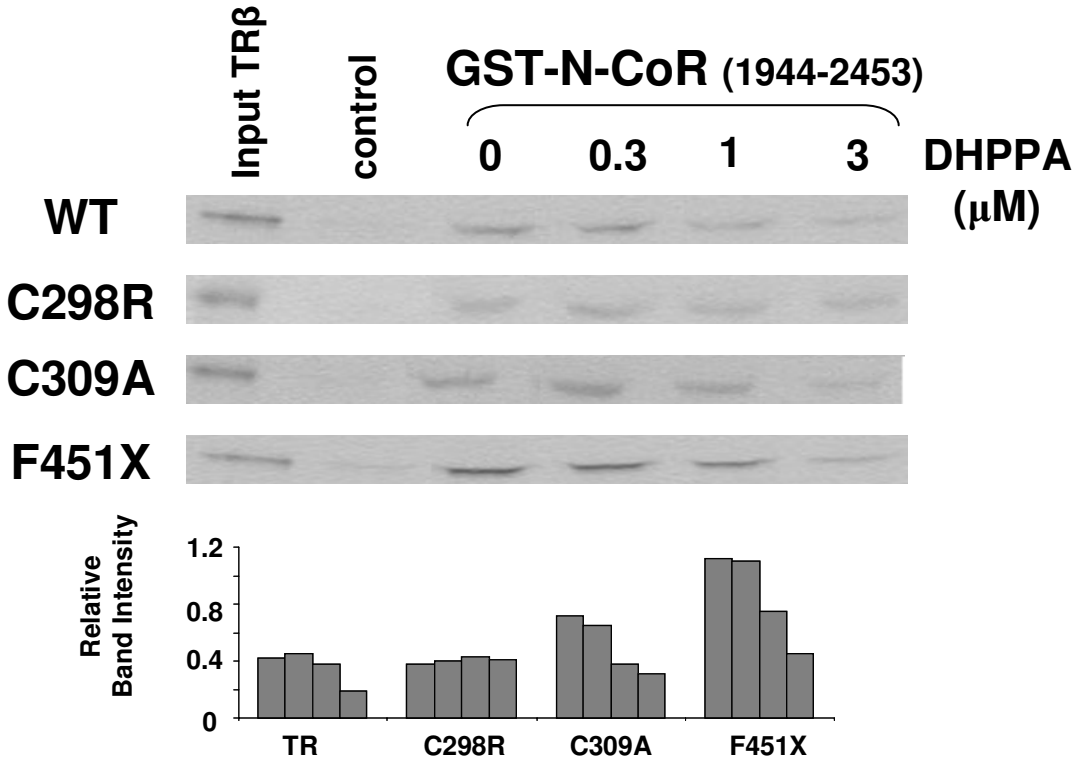
Input TRβ
control
GST-N-CoR (1944-2453)
0
0.3
1
3
DHPPA (μM)
WT
C298R
C309A
F451X
Relative Band Intensity
1.2
0.8
0.4
0
TR
C298R
C309A
F451X